



**HAL**  
open science

# Oxygenated terminals of milky sap of *Calotropis procera* transformed 1D ZnO structure to 0D nanoparticles for enhanced photocatalytic degradation of malachite green and methylene blue

Muhammad Ali Bhatti, Aneela Tahira, Ahmed Ali Hullio, Umair Aftab, Ayman Nafady, Brigitte Vigolo, Zafar Hussain Ibupoto

## ► To cite this version:

Muhammad Ali Bhatti, Aneela Tahira, Ahmed Ali Hullio, Umair Aftab, Ayman Nafady, et al.. Oxygenated terminals of milky sap of *Calotropis procera* transformed 1D ZnO structure to 0D nanoparticles for enhanced photocatalytic degradation of malachite green and methylene blue. *Journal of Materials Science: Materials in Electronics*, 2023, 34 (10), pp.929. 10.1007/s10854-023-10290-4 . hal-04222027

**HAL Id: hal-04222027**

**<https://hal.univ-lorraine.fr/hal-04222027>**

Submitted on 28 Sep 2023

**HAL** is a multi-disciplinary open access archive for the deposit and dissemination of scientific research documents, whether they are published or not. The documents may come from teaching and research institutions in France or abroad, or from public or private research centers.

L'archive ouverte pluridisciplinaire **HAL**, est destinée au dépôt et à la diffusion de documents scientifiques de niveau recherche, publiés ou non, émanant des établissements d'enseignement et de recherche français ou étrangers, des laboratoires publics ou privés.

**Oxygenated terminals of milky sap of calotropis procera transformed 1D ZnO structure to 0D nanoparticles for enhanced photocatalytic degradation of malachite green and methylene blue**

Muhammad Ali Bhatti<sup>a</sup>, Aneela Tahira<sup>c</sup>, Ahmed Ali Hullio<sup>b</sup>, Umair Aftab<sup>d</sup>, Ayman Nafady<sup>e</sup>, Brigitte Vigolo<sup>f</sup>, Zafar Hussain Ibupoto<sup>b</sup>

<sup>a</sup>Institute of Environmental Sciences, University of Sindh Jamshoro, 76080, Sindh Pakistan

<sup>b</sup>Institute of Chemistry, University of Sindh Jamshoro, 76080, Sindh Pakistan

<sup>c</sup>Institute of Chemistry, Shah Abdul Latif University Khairpur Mirs, Sindh, Pakistan

<sup>d</sup>Mehran University of Engineering and Technology, 7680 Jamshoro, Sindh Pakistan

<sup>e</sup>Department of Chemistry, College of Science, King Saud University, Riyadh 11451, Saudi Arabia

<sup>f</sup>Université de Lorraine, CNRS, IJL, F-54000 Nancy, France

**\*Corresponding authors:** Zafar Hussain Ibupoto

**Email:** [zaffar.ibhupoto@usindh.edu.pk](mailto:zaffar.ibhupoto@usindh.edu.pk)

**Abstract**

The use of plant extract for the synthesis of nanomaterials has been preferred over conventional growth techniques due to its safety, simple, ecofriendly, cost effective and biocompatibility properties. The present study includes environmentally friendly approach for synthesis of ZnO-NPs using milky sap of calotropis procera (CP) parts. The biosynthesized ZnO-NPs were investigated in terms of crystalline, morphology, and optical characterization. The CP has resulted spherical shaped oriented nanoparticles, hexagonal phase and significantly reduced crystallite size of -26.1 nm. The photodegradation of malachite green (MG) and methyl blue (MB) dye under the illumination of UV light was investigated using biosynthesized ZnO-NPs. The effect of different volume of milky sap of CP was considered as a point of care to demonstrate its role towards the enhancement of photodegradation effectiveness of ZnO against two different organic dyes like malachite and methylene blue owing their issues raised for aquaculture and worsen environmental impacts. The degradation of both dyes was followed by

pseudo first order kinetics and highest volume of milky sap of CP has given out high rate constant value. The degradation efficiency of milky sap of CP assisted ZnO nanostructures was found about 85.3% and 86.3% for MG and MB respectively. However, we studied the effect of pH of dye solution on the photocatalytic performance of ZnO and it has revealed highly enhanced degradation efficiency. The increased functionality of ZnO was connected to the reduced particle size, optical band gap, and tunable surface properties with the use of terminal oxygenated groups.

**Keywords:** Milky sap of CP, biosynthesis, ZnO nanostructures, photodegradation

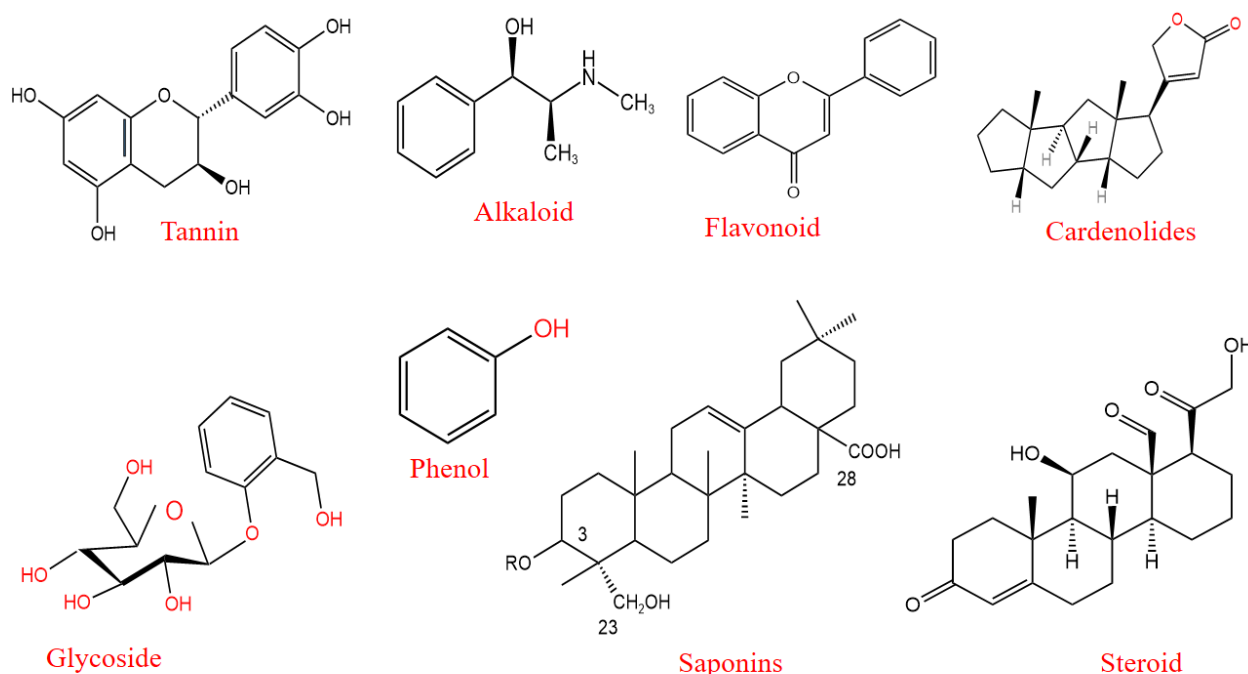
## **1. Introduction**

Synthetic dyes have been used extensively in various industries including textile, paper, plastic leather, food, and others. Many of them these dyes belong to azo compounds like methylene blue (MB), methyl orange (MO), Congo red (CR), direct black 38 (DB38), and malachite green (MG) containing chromophore ( $-N=N-$ ) in their chemical structures [1]. It has been remained a practice for the discard of these azo dyes directly or indirectly into environment and ecosystem of our water without or less likely treatment. Owing to their stable nature, they have been found hazardous and threat to life due to mutagenic and carcinogenic properties [2]. The stable nature of these dyes do not allow them for spontaneously degradation in the water, hence they have been causing pollution not for ecosystem of water but at the same time for our atmosphere, therefore the toxic effects on the aquatic life unavoidable. For these reasons, different wastewater treatment methods have been utilized and proposed [3-7]. The challenges faced by these established methods include the complicated working principle, high cost and some of them produces secondary class of pollutants during the degradation process. Therefore, it is very essential to realize new approaches with complementary technologies with low cost, environment friendly, ecofriendly, and highly efficient to transform these stable dyes into harmless minerals without producing the secondary pollutants.

Among these methods, the photocatalysis has been found the potential approach for the complete mineralization of these organic dyes into harmless products like  $H_2O$ , and  $CO_2$ . Today, the photocatalysis is strongly supported by the advancement in the field of material science due to extensive manipulation of wide range of materials at nanoscale dimension, hence vigorous efforts have been devoted to synthesizing and characterize for the wastewater treatment applications. It is the reason, wide range of nanostructured materials have been applied

particularly the semiconducting materials including TiO<sub>2</sub> [8], ZnO [9], Fe<sub>2</sub>O<sub>3</sub> [10], CdS [11], and ZnS [12] for the photocatalytic applications. Beside other semiconducting metal oxides photocatalysts, zinc oxide (ZnO) is intensively investigated for the photodegradation of diverse organic dyes due its significant catalytic activity, tunable optical band gap, low cost, easy to fabricate and ecofriendly. However, the potential emergence of ZnO as photocatalyst for the practical applications is restricted by the wide band gap, low density of catalytic sites and fast charge recombination rate of electron and holes [12]. Overcoming these main issues of ZnO for the photocatalytic applications, various efforts have been effectively taken into consideration such as adaption of new morphologies [9], use of new synthetic routes [9], engineering of optical band gap via efficient dopant, making composites systems, and using natural compounds from the plant extracts and biomass wastes as green methodology of preparation of ZnO nanostructures [13]. Recently, the green preparation strategy is being used with overwhelming, depicting its low cost, environment friendly, scale up, and avoiding the high consumption of toxic chemicals for the synthesis of ZnO nanostructures [14]. The plant extract is associated with the presence of large amounts of surface modifying agents, reducing agents, oxidizing agents, capping, and stabilizing agents which together play a vital role in controlling the size of nanostructured material, evolving the unique architecture of nanostructured morphologies [13-16]. For this purpose, the recent literature shows the intense use of wide range of plant extracts for the preparation of ZnO nanoparticles like *Azadirachta Indica (L)* [17], *Eucalyptus globulus (E. globulus)* [18], *Moringa Oliefera* leaf extract [19], *Cassia fistula* plant extract [20], *Citrus aurantifolia (lemon)* peel extract [21], leaf extract of *Calotropis Gigantea* [22], *Vitex negundo* leaf extract [23], *Caralluma Fimbriata* extract [24], and *Solanum nigrum* leaf extract [25]. Furthermore, Sharma *et al* (2016) and Dobrucka *et al* (2016) have synthesized ZnO nanoparticles using *Jacaranda mimosifolia* and *Trifolium pratense* flowers extracts [26, 27]. The synthesis of ZnO nanoparticles using *Lime* juice has been reported by Pandit 2017 [28]. And the Suresh *et al*, utilized the *Artocarpus Gomezianus (AG)* as fuel and followed by the combustion process for the preparation of ZnO nanoparticles [29], whereas Yuvakkumar *et al* [30] has taken *Nephelium lappaceum L. (rambutan)* peel extract for the biosynthesis of ZnO nanostructured material. *Calotropis procera* is a desert plant known in Greeco-Arab medicine as Ushar or Madar. Tropical and subtropical regions like Asia and Africa, have a large population of this plant [31]. The ancient Egyptians were aware of the plant's medical properties; excavations at Helwan in

Egypt revealed that the herb was used during the Neolithic period [32] In 'Berliner' papyrus, the plant is indicated for the treatment of nodular leprosy [33]. Since one decade, numerous scientific investigations have been conducted on different parts of this plant. According to Prakash et al. [34], *C. procera* negatively impacts both early and late pregnancy in rats. The extract of this plant extract is used as an anticancer [35] and nematocidal [36] properties. The flowers of *C. procera* have a highly substantial antibacterial and anti-inflammatory activity [37]. *Calotropis procera* (*C. Procera*, CP) is among the class of Apocynaceae and it is widely used for medicinal applications such as fever, diarrhea, asthma, painful muscle spasms and an aspiration and cleansing [38]. The CP is also applied for detoxify of the blood, making healthy hair, enhancing the liver function and to maintain the blood sugar levels. The CP plant is carrier of wide range of phytochemicals including triterpenoids, flavonoids, glycosides, anthocyanins,  $\alpha$ -amyrin,  $\beta$ -amyrin, lupeol,  $\beta$ -sitosterol, flavonols, mudarine and resins I [39]. The king draw was used to generate the molecular structure of various natural compounds of CP as shown in Scheme 1.



**Scheme 1:** Molecular structure of different chemical compounds carried by CP

A. Muthuvel, et al. is the one who utilized the CP flower extract for the preparation of  $\text{CeO}_2$  NPs and applied for the photodegradation of methyl orange. However, CP being the abundant desert and agriculture land plant around the world and carrying the favorable phytochemicals of milky

sap is not investigated and there is no report about the use of CP to improve to photocatalytic properties of ZnO material towards the photodegradation of malachite green (MG) and methylene blue (MB). Moreover, the role of different of volumes of CP on the structural disorder of ZnO and their role on the pH dependent photocatalytic functionality of MG and MB degradation in aqueous solution have never been studied and reported to date. Importantly, the role of terminated oxygen groups present in the biomass for the alteration of morphology from one dimensional (1D) to zero dimensional (0D) nanoparticles has not been highlighted and studied previously.

In this study, an ecofriendly, cost effective and rapid method for the synthesis of 0D ZnO nanoparticles using milky sap of CP was carried out. We have utilized milky sap of stem, flowers and leaves of CP for the preparation of ZnO nanostructures and studied their photocatalytic effectiveness during photodegradation of MB and MG under alkaline and acidic conditions. These observed findings propose a new functional aspect for the synthesis of ZnO nanostructures with outperform functionality under alkaline conditions and their suitability as an alternative photocatalyst for the practical applications.

## **2. Material and methods**

### **2.1. Material**

Zinc acetate dihydrate ( $\text{ZnC}_4\text{H}_6\text{O}_4$  Mm: 183.48 g/mol), ammonia aqueous solution (33%), ethanol ( $\text{C}_2\text{H}_5\text{OH}$ , 99%), sodium hydroxide (NaOH), hydrochloric acid (HCl, 37%), methylene blue (MB) and malachite green (MG) were bought from Merck and used as received with no additional sophistication. The deionized water was used to make a desired solution.

### **2.2. Milky sap collection from *Calotropis procera* and biosynthesis of ZnO nanostructures**

*Calotropis procera* (CP) is commonly known by sodom apple and belonging to apocynaceae family. The milky sap was collected from the various parts of CP including flower, stem and leaves. The CP plant was located at the mountain locality of University of Sindh jamshoro and prior to collection of milky sap, it was washed and cleaned several times with the deionized water. The volume of 50 mL of milky sap was obtained and used for the growth of ZnO nanostructures. The synthesis of ZnO nanostructures in the presence of milky sap of CP was performed by the solvothermal method. A solvothermal process is low cost, facile, ecofriendly and environment friendly, and can be used for the large scale synthesis of nanostructured

**materials.** In typical preparation process, we have used 2.22 g of zinc acetate dihydrate and 5 mL of 33% aqueous ammonia solution in 100 mL of the deionized water. At the same time, 15 mL of milky sap of CP was mixed with 20 mL of ethanol and homogenized mechanically. Then, milky sap dissolved into ethanol was added in the four beakers containing zinc precursor of 2.22 g of zinc acetate dihydrate and 5 mL of 33% aqueous ammonia with different volumes like 2 mL, 4 mL, 6 mL, and 8 mL respectively. The milky sap is carrying different types of stabilizing agents, capping agents and chelating agent like oxygen terminals which could bind effectively with zinc ions and played a dynamic role in the structure transformation and enhancement of photocatalytic properties of ZnO. For understanding the role of milky sap of CP, we have prepared the pure sample of ZnO under the same conditions without the use of milky sap. The solvothermal process was initiated by covering the growth solutions with aluminum sheet and left for chemical reaction at 95 °C for 5 hours. Afterwards, the white product of ZnO precipitates was settled at the bottom of each beaker and collected onto the ordinary filter paper and washed several times with the ethanol followed by deionized water. Then, the white product of ZnO was left to dry at 65 °C for 12 hours. Later, the white product of ZnO of each sample was kept in China clay made crucible and thermally treated at 250 °C for 3 hours in air. After the thermal combustion, ZnO samples were used for the structural, morphological, and photocatalytic applications.

### **2.3.Morphology, crystal phase and optical characterization of as biosynthesized ZnO nanostructures**

The crystalline phase and purity of as prepared ZnO nanostructures with milky sap of CP were explored by powder X-ray diffraction (XRD) technique with scanning two theta angle from 10° to 90° and X rays with a wavelength of 1.5406 Å were generated from Cu anode by applying potential of 45 kV with a current of 45 mA [40]. The crystalline size was estimated by using Scherrer equation ( $D = K \lambda / \beta \cos \theta$ ), here D is d- spacing of particular crystal planes, K is constant (0.9),  $\lambda$  as wavelength of used X-rays (1.5406 Å),  $\beta$  is the angular full width at half maximum in radians and  $\theta$  is the Bragg's angle. The morphology of milky sap assisted ZnO nanostructures was investigated by using low resolution scanning electron microscopy (SEM model JEOL JSM-5910). The SEM imaging was done with the accelerated voltage of 20 kV and prior to analysis the samples were coated with 5 nm gold coating in order to measure the well resolved images. The SEM imaging was collected with polaroid P/N 665 film [41, 42]. The

optical features about the biosynthesized were studied by employing UV-visible spectrophotometer (PE Lamda 365) with wavelength 200-800 nm range [43].

#### 2.4. Photocatalytic activity of biosynthesized ZnO nanostructures

The photodegradation was carried out with the use of 5 mg of different ZnO nanostructures obtained with milky sap of CP were mixed with dye solution, homogenized with in ultrasonic bath for 20 min in the dark. The placement of dye solution with ZnO nanostructures in ultrasonic bath was done in order to achieve the equilibrium of adsorption and desorption process. The photodegradation of both MB and MG dyes with milky sap assisted ZnO nanostructures was done under the illumination of ultraviolet of light. For comparison, the photodegradation of MB and MG with pure ZnO sample was also carried out. For the photocatalytic activity, various ZnO nanostructures were treated with MG dye concentration of  $10.96 \times 10^{-5} \text{M}$  and MB of  $3.12 \times 10^{-5} \text{M}$ . Then, 50 mL of each dye solution was taken and 5 mg of each sample of ZnO was added and stirred for 30 min to reach an adsorption-desorption equilibrium in the dark and we noticed that there was about 4-6 % adsorption and further no visible changes were noticed with naked eyes. The dyes solution with photocatalyst were placed in homemade UV light box consisting of six UV lamps of wavelength of (365 nm and power of 60 W). Afterwards, 2 mL of aliquots of dye solution was used in the cuvette and evaluated its absorption value by the UV-visible spectrophotometer (PE Lamda 365) for wavelength range from 250 to 750 nm. The process of each measurement was repeated for different intervals of time to monitor the degradation rate with the decrease in the absorbance for both MG and MB dyes under the illumination of UV light. The percent degradation was quantified by the following relationship:

$$\text{Photodegradation efficiency (\%)} = \frac{A_0 - A_t}{A_0} \times 100$$

Herein, the  $A_0$  and  $A_t$  were initial and after certain interval time dye absorption and same equation was used to evaluate the photocatalytic properties of pure ZnO and milky sap assisted

ZnO nanostructures. The dye degradation kinetics was studied through under given mathematical equation:

$$\ln \left( \frac{C_t}{C_o} \right) = kt$$

Whereas  $C_o$  and  $C_t$  are the dye initial concentration and after a specific time intervals for the illustration of rate constant (K) values in ( $\text{min}^{-1}$ ). The concentration of both dyes was expressed as mg/L. Furthermore, the effect of pH of dye solution on the degradation rate was studied using different ZnO samples. The pH of dye solution was adjusted by the use of aqueous solutions of 0.2M NaOH and HCl.

### **3. Result and discussion**

#### **3.1. Crystal phase, morphology and optical studies of milky sap of CP assisted ZnO nanostructures**

Crystal phase information was verified by the distinctive reflection patterns of biosynthesized ZnO nanostructures using powder XRD technique as shown in Figure 1. The XRD reflections were measured for the four samples of ZnO obtained with 2, 4, 6 and 8 mL of milky sap of CP and pure ZnO as shown in Figure 1. The observed reflections were well matched with the hexagonal phase of ZnO with typical wurtzite structure as reported previously [44]. Various XRD reflections were identified at wide range of two theta angle as shown herein at  $2(\theta^{\circ})$   $36.619^{\circ}$ ,  $34.335^{\circ}$ ,  $36.100^{\circ}$ ,  $47.367^{\circ}$ ,  $56.313^{\circ}$ ,  $62.645^{\circ}$ ,  $66.033^{\circ}$ ,  $67.641^{\circ}$ ,  $68.737^{\circ}$ ,  $72.362^{\circ}$  and  $76.588^{\circ}$  corresponded to crystal plane including (100), (002), (101), (102), (110), (103), (200), (112), (201), (004) and (202) respectively. All the noticed XRD reflections were further supported by the standard JCPDS card (01-079-0208). There have been no additional reflections which could not be labelled, confirming the high purity of as prepared ZnO samples. The relative intensity of (101) crystal plane was decreased with increasing amount of milky sap of CP, suggesting that the alteration of one dimensional nanostructures into heterogeneous structure due to driving role of oxygenated and hydroxyl groups of milky sap of CP. These oxygenated groups result the diverse and multidirectional approach of nucleation during the growth process, consequently the transformation of morphology was expected as proven by SEM analysis. Interestingly, the shift in the two theta along the (100) crystal plane was noticed as shown in

Figure 1b. This is connected to the wide range of polymeric biomolecules from milky sap of CP which created stress on the crystal orientation, hence shift towards right angle was observed as shown in Figure 1b. The induction of shift in two theta could cause the defects in the crystal arrays and introduced the imperfection in the crystal arrays of ZnO [44]. Moreover, the XRD results were used to describe the average crystallite size of biosynthesized ZnO nanostructures using Scherrer equation. The calculations of average crystallite size of different samples of ZnO prepared with 2, 4, 6 and 8 mL of milky sap of CP and pure ZnO were found in the order as 30.7 nm, 28.9 nm, 27.5 nm, 26.1 nm and 32.6 nm respectively as shown in Figure 1c. It is obvious that the 8 mL of milky sap of CP resulted the lowest average crystallite size of ZnO owing to the high density of oxygenated terminal groups which reduced the size of crystal. According to M.G Demissie, et al. the average crystal size of biosynthesized ZnO NPs has decreased with increasing volume of plant extract. This is because of the variation in the amount of effective capping and stabilizing agents which controlled on the size of nanoparticles, and avoided the possibility of aggregation, hence size of ZnO nanoparticles was decreased [45]. Furthermore, the morphology of as prepared ZnO nanostructures with various volumes of milky sap of CP was also examined using low resolution scanning electron microscopy (SEM) as depicted in the Figure 2. The pure ZnO was identified with typical one dimensional (1D) nanorod like morphology with obvious hexagonal faces, however they were found randomly oriented with high degree of size heterogeneity as shown in Figure 2a. The milky sap of CP has shown the dynamic contribution towards the transformation of 1D nanorod into zero dimensional (0D) rounded particle like structure with dimension of 400-600 nm. The increasing volume of milky sap has shown the significant indicators about the formation of special particles like morphology, and it could be attributed to the wide range of oxygenated terminal groups from the different natural compounds of milky sap. They have allowed the easy access to the zinc ions for binding and the hydrophobic part of each molecule have evolved the morphology into spherical shape. These oxygenated groups could be responsible for the new ways of crystal orientation during the growth process, hence we have noticed the complete transformation of nanorod like morphology into spherical particles [46, 47]. These observations could be supported from the XRD results in terms of change in the intensity of reflections which enabled the crystal orientation in the multiple directions in the presence of milky sap of CP as shown in Figure 2b-e. Previously, it has been reported that the morphology of nanostructured material is highly dependent on the nature

biomolecules present in the biomass of plants [48]. Additionally, it has been described in the literature that the spherical morphology is more likely useful for the antibacterial activity as it can easily go inside the bacterial strains and thereby show an effectiveness to kill biological cell [49]. On the basis of morphological characterization about the biosynthesized material, a hypothesis for the formation mechanism of nanoparticles is depicted in scheme 2. Given that *C. procera* extract is the abundant source of phytochemicals and many of them are rich with terminated atoms with lone pair which could effectively bound with the  $Zn^{2+}$  ions during hydrothermal process. Then, the kinetics of zinc ions binding with hydroxyl groups could be well controlled, hence shaping the structure from nanorods to nanoparticles. The availability of capping agents and chelating agents from milky sap of CP ultimately supported for the formation of nanoparticles [50].

The elemental information was verified by measuring the energy dispersive spectroscopy spectra (EDS) for each sample of ZnO prepared with, 2, 4, 6 and 8 mL of milky sap of CP as shown in Figure 3. Except pure sample of ZnO which only consists Zn and O as main elements. However, the milky sap assisted ZnO nanostructures do not only contain Zn, and O but at the same time Cl, S, C and Mg were also detected as shown in Figure 3 and such elemental chemical composition of milky sap of CP is reported elsewhere. The optical characterization in terms of optical band gap determination was also carried out to know the influence of milky sap of CP on the tuning the band gap, hence UV-visible absorbance spectra were measured as shown in Figure 4. The band gap calculations were done by extra plotting of  $(\alpha h\nu)^2$  plot versus  $(h\nu)$  photon energy. Herein,  $\alpha$  is known as absorption coefficient and it can be determined from the absorbance spectra by employing the Kubelka – munk theory, and  $h$  is the plank's constant,  $\nu$  is frequency of used photons [51]. The linear part after extrapolation of  $(\alpha h\nu)^2$  versus photon of energy  $(h\nu)$  gives out the value of optical band gap as shown in Figure 4. The obtained optical band gap for pure ZnO sample was observed around 3.34 eV, and the ZnO material prepared with 2, 4, 6 and 8 mL of milky sap of CP was estimated as 2.90 eV, 2.86 eV, 2.83 eV and 2.77 eV respectively. The band gap of milky sap assisted ZnO nanostructures was significantly reduced, revealing an outstanding role of variety of biomolecules from the CP affecting the optical features of as prepared material. The validation of band calculations of pure ZnO of 3.34 eV in this study could be verified from published works [44]. Furthermore, it should be noted in the literature that narrowing band gap may be caused by the loading of the dopant into ZnO,

creation of O and Zn vacancies, improved crystal quality at higher annealing and other factors[52]. We have already observed from EDS analysis that there is presence of Cl, S, C and Mg possibly they have been added into the crystal of ZnO, consequently the optical band gap was reduced.

### **3.2. Photocatalytic applications of as prepared ZnO nanostructures with milky sap of CP**

#### **a. MG degradation**

The photocatalytic applications of as biosynthesized ZnO nanostructures were chosen on two aspects one as the wastewater treatment and its environmental impacts and other is the water pollution causing many issues for the aquatic life especially the aquaculture systems. Hence, we have applied the newly modified ZnO nanostructures on the MB and MG for the evaluation of their photocatalytic effectiveness. First, we have examined the photodegradation of MG using  $10.96 \times 10^{-5} \text{M}$  in aqueous solution against the pure ZnO and biosynthesized ZnO samples with 2, 4, 6 and 8 mL of milky sap of CP under the illumination of UV light. The absorbance spectra of MG using pure ZnO as photocatalyst were recorded with different intervals of time like 25, 50, 75, 100, 125 and 150 min as enclosed in Figure 5a. The absorbance spectra were measured with the gap of 25 min as shown in Figure 5a. It is obvious that the relative decrease in the absorbance is limited, suggesting the poor performance of pure ZnO, owing to its wide band gap and the fast charge recombination of electron and holes during the photocatalysis process as previously described by several studies [53-55]. The degradation kinetics was also described by pseudo first order kinetics as illustrated in Figure 5b and the ratio of dye concentration after certain time of degradation process and the initial dye concentration was also measured as shown in Figure 5c, indicating the pseudo first order kinetics which is mainly governed by the concentration of MG. The degradation efficiency of pure ZnO was also investigated against the degradation of MG and identified by a very low of 31.3% as shown in Figure 5d and describing the solid reasons for the manipulation of pure ZnO properties by adapting new methodologies for improvement in the photocatalytic properties of ZnO. Similarly, pure ZnO was used for the photodegradation of MB and the obtained UV-visible absorbance spectra, reaction kinetics and

degree efficiency studies are enclosed in Figure 6a-d. Again, the performance of pure ZnO was found limiting and could not be useful for the practical applications.

Because the pure ZnO has limited photocatalytic activity and it has very less like potential to be used for practical applications of wastewater treatment in its pure form [53], therefore new roadmaps are highly needed based on ZnO by enhancing its photocatalytic properties for the development of real time photocatalysts in the near future. This is the reason, we have used the natural source of desert plant CP and it is widely distributed around the world, but its utilization towards photocatalytic applications is limited despite it carries wide range natural compounds including reducing agents, stabilization agents, capping agents and oxygen terminated groups for the evolution of surface morphology of ZnO nanostructures and modification of its optical properties. The milky sap of CP with different volumes like 2, 4, 6 and 8 mL were used to study the structural disorder, optical characteristics variations and the degradation effectiveness of ZnO nanostructures as shown in Figure 7. It can be visualized that the absorbance of MG decreased very sharply with the use ZnO samples prepared with different amounts of milky sap of CP. This confirms that the presence of natural products in the milky sap of CP have shown an excellent role to drive degradation rate swiftly as shown in Figure 7. Obvious role of 8 mL of milky sap of CP on the enhancement of photocatalytic of properties could be seen from Figure 7d. The estimated values of kinetic parameters of MG degradation are enclosed in Table 1 and they were obtained from the plot's  $\ln(C_0/C_t)$  versus time as shown in Figure 8a. The degradation kinetics of MG was described by the pseudo first order kinetics as indicated by the  $(C_t/C_0)$  of MG as illustrated in Figure 8b. The degradation percentage of various of samples of ZnO prepared with 2, 4, 6 and 8m mL of milky sap of CP was found as 47.8%, 66.4%, 78.5% and 85.3% as shown in Figure 8c respectively. From the degradation efficiency analysis, it is worth to note that the 8mL of milky sap of CP has demonstrated the highest value among the 2, 4 and 6 mL of milky sap of CP, revealing that it contains higher amount of natural compounds which together drive the degradation process very efficiently. These observations suggest that the 8 mL of milky sap of CP has offered high reduction in the optical band gap, high enhancement in the catalytic sites of ZnO, and high provision of electron and hole pairs during the photocatalysis with minimum charge recombination rate. The high generation of electrons and holes offers the large number of production of radicals like  $^{\circ}\text{OH}$  and  $^{\circ}\text{O}_2^-$  to degrade MG very effectievly and efficienctly.

## **b. Degradation of MB**

Furthermore, the photodegradation of MB was performed with the use of biosynthesized ZnO nanostructures in the presence of 2, 4, 6 and 8 mL of milky sap of CP. Before, the degradation of MB, the absorbance spectrum of bare dye was taken as shown in Figure 9 and it is shown by the absorbance bands in the region of 664 and 612 nm, indicating the typical sulfur-nitrogen conjugate bonding features and they have been labeled as the chromophoric groups within the MB molecular structure [56]. It has been observed that the intensity of both peaks should decrease once the degradation process is started, would confirm the cleavage of sulfur-nitrogen conjugate bonding sites and further demethylation could result into other intermediates [57, 58]. ZnO nanostructures synthesized with milky sap of CP were tested in MB dye solution  $3.12 \times 10^{-5}$  M the use of 5 mg of each photocatalyst under the illumination of UV light. The UV-visible absorbance spectra of MB under the treatment of various ZnO samples were measured the time interval of 15, 30, 45, 60, 75, 90, 105, 120 and 135 min, each measurement with time gap of 15 min as enclosed in Figure 10. The sharp decrease in the absorbance was observed with increasing amount of volume of milky sap of CP during the synthesis of ZnO nanostructures as shown in Figure 10a-d. It is clear, that the 8 mL like in case of MG, has shown dominant role in degrading the MB as well as shown in Figure 10d. The kinetics was also examined about the degradation of MB under the influence of biosynthesized ZnO nanostructures as given in Table 1 and from the kinetics parameters it is confirmed that photodegradation was followed by pseudo first order kinetics and it is only governed by the decrease in the absorbance of MB. The kinetics study of MB degradation is illustrated by Figure 11a,b. The relative degradation efficiency of various samples of ZnO synthesized with 2, 4, 6 and 8 mL of milky sap of CP is enclosed in Figure 11c and it was noticed in the order 36.9%, 51.0%, 62.4% and 86.32% respectively. These findings again, confirm that the morphology, optical band gap reduction, small crystallite size and surface modified features dependence performance of biosynthesized towards the degradation of MB in aqueous solution.

### **3.3. Effect of pH of MG and MB dye solution on the photocatalytic properties of ZnO nanostructures**

The effect of pH of dye solution on the performance evaluation of biosynthesized ZnO nanostructures was evaluated for the samples prepared with 8 mL of milky sap of CP using a  $8.22 \times 10^{-5}$  M MG as shown in Figure 12. The pH of bare  $8.22 \times 10^{-5}$  M MG solution was 6.3. The

pH of  $8.22 \times 10^{-5}$  M MG was adjusted with the use of 0.2 M NaOH and HCl solutions and 5 mg of sample of biosynthesized ZnO nanostructures was mixed with the MG dye solution and the pH of dye solution was used like 4, 8, and 10 as shown in Figure 12a-c. The well adsorption and desorption equilibrium were achieved by mechanical stirring in dark. Afterwards, the pH-maintained dye solutions with 5 mg of each sample ZnO were irradiated with UV light and analyzed for the decrease in the absorbance of UV light. The pH 4 of MG dye solution related decreases in the absorbance is enclosed in the Figure 12a. It is highly observed that the acidic pH of MG dye solution has shown the limiting decrease in the absorbance, indicating the unfavorable dye degradation due to the low density of radicals like hydroxyl or peroxide in the acidic solution, hence poor performance of degradation was noticed. The pH 4 of MG was changed to 4.3 during the degradation process. We have also studied the kinetics dye degradation in the pH 4 and observed performance is defined by the low values of rate constant and the reaction kinetics was predominated by pseudo-order kinetics as shown in Figure 12d. The most noticed observation is about the ZnO sample prepared with 8 mL of milky sap of CP that has shown the enhanced degradation rate. The degradation of MG under acidic environment of MG dye solution was found as 55.1% for the time period of 90 min for different samples of ZnO with the use of 8 mL of milky sap assisted nanostructures as shown in Figure 12f. Furthermore, the pH 8 of MG dye solution was used to illustrate the effect of pH on the photocatalytic performance of ZnO nanostructures obtained with 8 mL of milky sap of CP as shown in Figure 12b. It can be seen the activity of material is enhanced with increase in the pH of dye solution from slightly alkaline conditions. We also studied the kinetics of degradation of MG under slightly alkaline conditions and analysis is enclosed in the Figure 12e. The kinetic study has revealed better reaction rate and 8 mL of milky sap assisted ZnO nanostructured has demonstrated the significant rate constant value as shown in Figure 12e. The relative degradation efficiency of ZnO sample prepared with 8 mL of milky sap of CP was observed as 92.6% as enclosed in Figure 12f. It was noticed that the pH 8 of MG dye solution was changed to 8.3 after the degradation process. At the same time, have investigated the higher alkaline pH of 10 of MG dye solution against the ZnO nanostructures synthesized with 8 mL of milky sap of CP as shown in Figure 12 c with contributed decrease in the absorbance of light. These results of pH 10 strongly suggest the outperform functionality of ZnO as photocatalyst against MG dye degradation. This is because the higher alkaline conditions offer high amount of hydroxyl

groups which played a dominant role in degrading the MG as a main radical component as shown in Figure 12c. Similarly, the reaction kinetics was studied and described by the pseudo-order kinetics and mainly governed by the concentration of MG as shown in Figure 12e. The degradation of efficiency was found as 93.4 % for various samples of ZnO using 8 mL of milky sap of CP for the time period of 20 min as enclosed in Figure 12f. The high performance at pH 10 is attributed to the point zero charge as previously observed by several studies [59, 60]. This is because at alkaline pH, the surface of ZnO is decorated with negatively charged hydroxyl which favored the degradation kinetics [61]. However, under the acidic conditions the surface of ZnO is rich with positively charge of hydronium ions which repelled the cationic dyes like MG, hence poor performance was observed at pH 4 of MG dye solution [59]. The pH 10 of MG dye solution was also slightly varied from 10 to 10.4 during the degradation process. Additionally, it has been shown that the slow degradation kinetics under acidic situations is attributed to the corrosive nature dye solution for the etching of ZnO [62, 63]. At the same time, the influence of pH of MB dye solution was also studied with the ZnO sample prepared with 8 mL of milky sap of CP and its degradation kinetics and efficiency were studied as shown in Figure 13a-f. Both the rate constant, and degradation efficiency were highly enhanced by the change in the pH of dye solution. The degradation kinetics was following pseudo-order kinetics and suggesting that the MB concentration is the effecting the rate of degradation. The summary of obtained results in terms of rate constant with the use of different volumes of milky sap of CP and the effect of pH of dye solution are given in Table 1. Both the volume of milky sap of CP and pH of dye solution were found the key indicators for enhanced performance of as prepared ZnO sample with 8m mL. After the degradation process, the pH 4, 8 and 10 was slightly increased 4.3, 8.2 and 10.3 respectively.

### 3.4.Generalized photodegradation mechanism

The photodegradation is accompanied by photoexcitation, migration of charges, charge separation and redox process on the surface of photocatalyst as already described [64]. The reactive species like ( $h^+$ ,  $OH^-$  and  $^{\bullet}O_2^-$ ) have been observed when photons of particular light are striking on the surface of photocatalyst. For the possible illustration of possible photodegradation mechanism by considering the reported research works [67-72]. At the time of irradiation of light, the electrons are moving from valence band to conduction band of , thereby creating a

hole in the valence band as shown in Scheme 3. This scenario offers the simultaneous production of electron and hole pairs and they have been interacting with the water and generate wide range of oxidizing radicals like hydroxyl ( $^{\circ}\text{OH}$ ) and superoxide ( $^{\circ}\text{O}_2^-$ ) [67-72]. Later, these highly active radicals participate in the degradation of organic pollutants like MB and MG [65]. The photodegradation of organic dyes using nanostructured materials is mainly governed by the dimension, shape orientation and surface properties of as prepared nanostructured materials [67]. The performance evaluation of presented work was compared with the previous studies in terms of degradation efficiency, degradation time and synthesis method as given in Table 2. It is obvious that the presented method of material synthesis is low cost, green, ecofriendly, environment friendly, scale up production of material and the degradation performance is either superior or equal to many of the recently reported works. The improved performance of biosynthesized ZnO could be related to presence of the impurities like Mg, Cl, C and S in the samples using milky sap of CP, and it has shown that the relative amount of them is increasing with increasing amount of milky sap of CP. These impurities may play role in making the crystal defects, narrowing the optical band gap and variation in the surface chemical composition of ZnO, consequently they have shown favorable role towards the dye degradation as confirmed by the use of higher volume of milky sap of CP.

#### 4. Conclusions

In summary, we have prepared ZnO nanostructured materials using milky sap of CP through solvothermal process followed calcination in air. The XRD study has verified the alteration in the orientation of crystal via decrease in the reflection intensities and suggested the structural transformation of ZnO nanorod. XRD study has revealed the decrease in the crystallite size of ZnO. Furthermore, it was verified by the SEM analysis and typical 1D nanorod like morphology was transformed into 0D spherical particle due to the high density of surface transforming oxygenated terminal group's presence in the milky sap of CP. The role of milky sap of CP was found highly dominant on the optical properties of ZnO which was clearly defined by the reduction in the band gap at higher amounts of 8 mL of milky sap of CP used for the growth of ZnO nanostructures. The catalytic activity of as prepared ZnO nanostructures was evaluated against the MG and MB under the illumination of UV light and variation in the pH of dye

solutions. The photodegradation efficiency of MG and MB was observed as 94.1% at 20-120 min and 93.9% of the MB at 15-135 min respectively. The reaction kinetics of both dyes degradation was confirmed by the pseudo order kinetics. These obtained values of structural disorder, optical band gap and the photocatalytic of ZnO, suggesting the potential and promising features of milky sap of CP for other metal oxides and related nanostructured materials to drive their enhanced functionality towards energy and environment related applications.

### **Author contributions**

Muhammad Ali Bhatti, did synthesis of ZnO nanostructures and evaluate the partial photocatalytic properties

Aneela Tahira, did XRD analysis

Ahmed Ali Hullio, did analysis of obtained photodegradation results

Umair Aftab, did optical bandgap analysis

Ayman Nafady, partially supervised the work and edit the draft of manuscript

Brigitte Vigolo, did the SEM analysis and edit the draft of paper

Zafar Hussain Ibupoto, supervised the work and wrote the first draft of manuscript

### **Acknowledgement**

The authors extend their sincere appreciations to Researchers Supporting Project number (RSP2023R79), King Saud University, Riyadh, Saudi Arabia, for partial funding of this work.

### **Conflict of Interest**

Authors declare no conflict of interest in the presented research work

### **Data Availability Statement**

Data will be made available on reasonable request

## 5. References

- [1]. H.Y. Zhu, R. Jiang, Y.Q Fu, Y.J Guan, J. Yao, L. Xiao, G. Zeng , Effective photocatalytic decolorization of methyl orange utilizing TiO<sub>2</sub>/ZnO/ chitosan nanocomposite films under simulated solar irradiation. *Desalination*, **286**, 41-48 (2012)
- [2]. N. Mathur, P. Bhatnagar, P. Sharma, Review of the mutagenicity of textile dye products. *Universal Journal of Environmental Research & Technology*, **2**, 1-18 (2012)
- [3]. R. Kumar, G. Kumar, A. Umar, ZnO nano-mushrooms for photocatalytic degradation of methyl orange. *Materials Letters*, **97**,100-103 (2013)
- [4]. M. Arab Chamjangali, G. Bagherian, B. Bahramian, B. Fahimi Rad, Synthesis and application of multiple rods gold–zinc oxide nanostructures in the photocatalytic degradation of methyl orange. *International Journal of Environmental Science and Technology*, **12**,151-160 (2015).
- [5]. N.Z. Razali, A.H. Abdullah, M.. Haron, Degradation of methyl orange mediated by CuO-doped ZnO photocatalysts *Environmental Engineering & Management Journal (EEMJ)*, **10**, 1523–1528 (2011).
- [6]. N. Tripathy, R. Ahmad, J.E. Song, H.A. Ko, Y.B. Hahn, G. Khang, Photocatalytic degradation of methyl orange dye by ZnO nanoneedle under UV irradiation. *Materials Letters*, **136**, 171-174 (2014).
- [7]. F. Tian, Z. Wu, Q. Chen, Y. Yan, G. Cravotto, Z. Wu, Microwaveinduced crystallization of AC/TiO<sub>2</sub> for improving the performance of rhodamine B dye degradation. *Applied Surface Science*, **351**, 104-112 (2015).
- [8]. D. Liu, Z. Wu, F. Tian, B.C. Ye, Y. Tong, Synthesis of N and La codoped TiO<sub>2</sub>/AC photocatalyst by microwave irradiation for the photocatalytic degradation of naphthalene *Journal of Alloys and Compounds*, **676**, 489-49 (2016).
- [9]. S. Chidambaram, B. Pari, N. Kasi, S. Muthusamy, ZnO/Ag heterostructures embedded in Fe<sub>3</sub>O<sub>4</sub> nanoparticles for magnetically recoverable photocatalysis . *Journal of Alloys and Compounds*, **665**, 404-410 (2016).

- [10]. Y. Liu, L. Yu, Y. Hu, C.F. Guo, F.M. Zhang, X.W. Lou, A magnetically separable photocatalyst based on nest-like  $\gamma$ -Fe<sub>2</sub>O<sub>3</sub>/ZnO double-shelled hollow structures with enhanced photocatalytic activity. *Nanoscale* **4**, 183–187 (2012).
- [11]. A. Vázquez, D.B Hernández-Uresti, S. Obregón, Electrophoretic deposition of CdS coatings and their photocatalytic activities in the degradation of tetracycline antibiotic. *Appl Surf Sci* **386**, 412–417 (2016).
- [12]. D. Pathania, D. Gupta, H. Ala'a, G. Sharma, A. Kumar, M. Naushad, T. Ahamad, S.M. Alshehri, Photocatalytic degradation of highly toxic dyes using chitosan-g-poly (acrylamide)/ZnS in presence of solar irradiation. *J Photochem Photobiol A*, **329**, 61–68 (2016).
- [13]. K. Govindaraju, S. Khaleel Basha, V. Ganesh Kumar, G. Singaravelu, Silver, gold and bimetallic nanoparticles production using single-cell protein (*Spirulina platensis*) Geitler. *J. Mater. Sci.* **43**, 5115–5122 (2008).
- [14]. G. Scarano, E. Morelli, Properties of phytochelatin-coated CdS nanocrystallites formed in a marine phytoplanktonic alga (*Phaeodactylum tricornutum*, Bohlin) in response to Cd. *Plant Sci.* **165**, 803–810 (2003).
- [15]. M.F. Lengke, M.E. Fleet, G. Southam, Biosynthesis of silver nanoparticles by filamentous cyanobacteria from a silver (I) nitrate complex. *Langmuir* **23** (5) 2694-2499 (2007) <https://www.ncbi.nlm.nih.gov/pubmed/17309217>.
- [16]. A. Muthuvel, M. Jothibas, C. Manoharan, S.J. Jayakumar, Synthesis of CeO<sub>2</sub>-NPs by chemical and biological methods and their photocatalytic, antibacterial and in vitro antioxidant activity. *Research on Chemical Intermediates*, **46**, 2705-2729 (2020).
- [17]. K. Elumalai, S. Velmurugan, Green synthesis, characterization and antimicrobial activities of zinc oxide nanoparticles from the leaf extract of *Azadirachta indica* (L.). *Appl. Surf. Sci.* **345**, 329–36 (2015).
- [18]. B. Siripireddy, B.K. Mandal, Facile green synthesis of zinc oxide nanoparticles by *Eucalyptus globulus* and their photocatalytic and antioxidant activity. *Adv. Powder Technol.* **28**, 785–97 (2017).
- [19]. K. Elumalai, S. Velmurugan, S. Ravi, V. Kathiravan, S. Ashokkumar, Green synthesis of zinc oxide nanoparticles using *Moringa oleifera* leaf extract and evaluation of its

- antimicrobial activity Spectrochim. Acta - Part A Mol. Biomol. Spectrosc. **143**, 158–64 (2015).
- [20]. D. Suresh, P.C. Nethravathi, H. Rajanaika, H. Nagabhushana, S.C Sharma, Green synthesis of multifunctional zinc oxide (ZnO) nanoparticles using Cassia fistula plant extract and their photodegradative, antioxidant and antibacterial activities. Mater. Sci. Semicond. Process. **31**, 446–54 (2015).
- [21]. H. Çolak, E. Karaköse, Green synthesis and characterization of nanostructured ZnO thin films using Citrus aurantifolia (lemon) peel extract by spin-coating method. J. Alloys Compd. **690**, 658–62 (2017).
- [22]. S.K. Chaudhuri, L. Malodia, Biosynthesis of zinc oxide nanoparticles using leaf extract of Calotropis gigantea: characterization and its evaluation on tree seedling growth in nursery stage. Appl. Nanosci. **7**, 501–12 (2017)..
- [23]. S. Ambika, M. Sundrarajan, Green biosynthesis of ZnO nanoparticles using Vitex negundo L. extract: Spectroscopic investigation of interaction between ZnO nanoparticles and human serum albumin. J. Photochem. Photobiol. B Biol. **149**, 143–8 (2015).
- [24]. P. Mishra, P. Singh, H.P. Nagaswarupa, S.C. Sharma, Y.S. Vidya, S.C. Prashantha, H. Nagabhushana, K.S Anantharaju, S. Sharma, L. Renuka, Caralluma fimbriata extract induced green synthesis, structural, optical and photocatalytic properties of ZnO nanostructure modified with Gd. J. Alloys Compd. **685**, 656–69 (2016).
- [25]. M. Ramesh. M. Anbuvaran, G. Viruthagiri, Green synthesis of ZnO nanoparticles using Solanum nigrum leaf extract and their antibacterial activity Spectrochim. Acta—Part A Mol. Biomol. Spectrosc. **136**, 864–70 (2015).
- [26]. D. Sharma, M.I. Sabela, S. Kanchi, P.S. Mdluli, G. Singh, T.A. Stenström, K. Bisetty, Biosynthesis of ZnO nanoparticles using Jacaranda mimosifolia flowers extract: synergistic antibacterial activity and molecular simulated facet specific adsorption studies. J. Photochem. Photobiol. B Biol. **162**, 199–207 (2016).
- [27]. R. Dobrucka, J. Długaszewska, Biosynthesis and antibacterial activity of ZnO nanoparticles using Trifolium pratense flower extract. Saudi J. Biol. Sci. **23**, 517–23 (2016).
- [28]. S.P. Hinge, A.B. Pandit, Solar-assisted synthesis of ZnO nanoparticles using lime juice: a green approach. Adv. Nat. Sci.: Nanosci. Nanotechnol. **8**, 045006–20 (2017).

- [29]. D. Suresh, R.M. Shobharani, P.C. Nethravathi, M.A. Pavan Kumar, H. Nagabhushana, S.C. Sharma, *Artocarpus gomezianus* aided green synthesis of ZnO nanoparticles: luminescence, photocatalytic and antioxidant properties *Spectrochim. Acta - Part A Mol. Biomol. Spectrosc.* **141**, 128–34 (2015).
- [30]. R. Yuvakkumar, J. Suresh, A.J. Nathanael, M. Sundrarajan, S.I. Hong, Novel green synthetic strategy to prepare ZnO nanocrystals using rambutan (*Nephelium lappaceum* L.) peel extract and its antibacterial applications. *Mater. Sci. Eng.C.***41**, 17–27 (2014).
- [31]. A.G. Millar, M. Morris, *Plants of Dhofar; The Southern Region of Oman, Traditional, Economic and Medicinal Uses*. The office of the Advisor for Conservation of the Environment, Diwan of Royal Court Sultanate of Oman, 42, (1987).
- [32]. A.M. Greiss. Elhamy, *Anatomical Identification of plant remains and other materials from (1) El-Omari excavation at Helwan from the first dynasty*. *Bull Inst. Egypt.* **36**, 227-235 (1955).
- [33]. B.A. Ebbell, contribution to the earliest history of leprosy. *Int. J. Leprosy.* **3**, 257-263 (1935).
- [34]. Prakash, A.O., Gupta, R.B. and Mathur, R. Effect of oral administration of forty two indigenous plants extracts on early and late pregnancy in albino rats. *Probe*, **27**, 315-323 (1978).
- [35]. S.M.H. Ayoub, D.G.I. Kingston, Screening of plants used in Sudan folk medicine for anticancer activity. *Fitoterapia*, **52**, 281-284 (1981).
- [36]. S.N. Nandal, D.S. Bhatti, Preliminary screening of some weeds and shrubs for their nematocidal activity against *Meloidogyne javanica*. *Indian J. Nematol.*, **13**, 123-127 (1983).
- [37]. N. Mascolo, R. Sharma, S.C. Jain, F. Capasso, *Ethnopharmacology of calotropis procera flowers*. **22**, 211-221 (1988).
- [38]. A. Muthuvel, M. Jothibas, V. Mohana, C. Manoharan, Green synthesis of cerium oxide nanoparticles using *Calotropis procera* flower extract and their photocatalytic degradation and antibacterial activity. *Inorganic Chemistry Communications*. **119**, 108086 (2020).
- [39]. R.P. Mali, P.S. Rao, R. Jadhav, A review on pharmacological activities of *calotropis procera*. *J. Drug. Deliv. Ther.* **9**, 947–951 (2019).

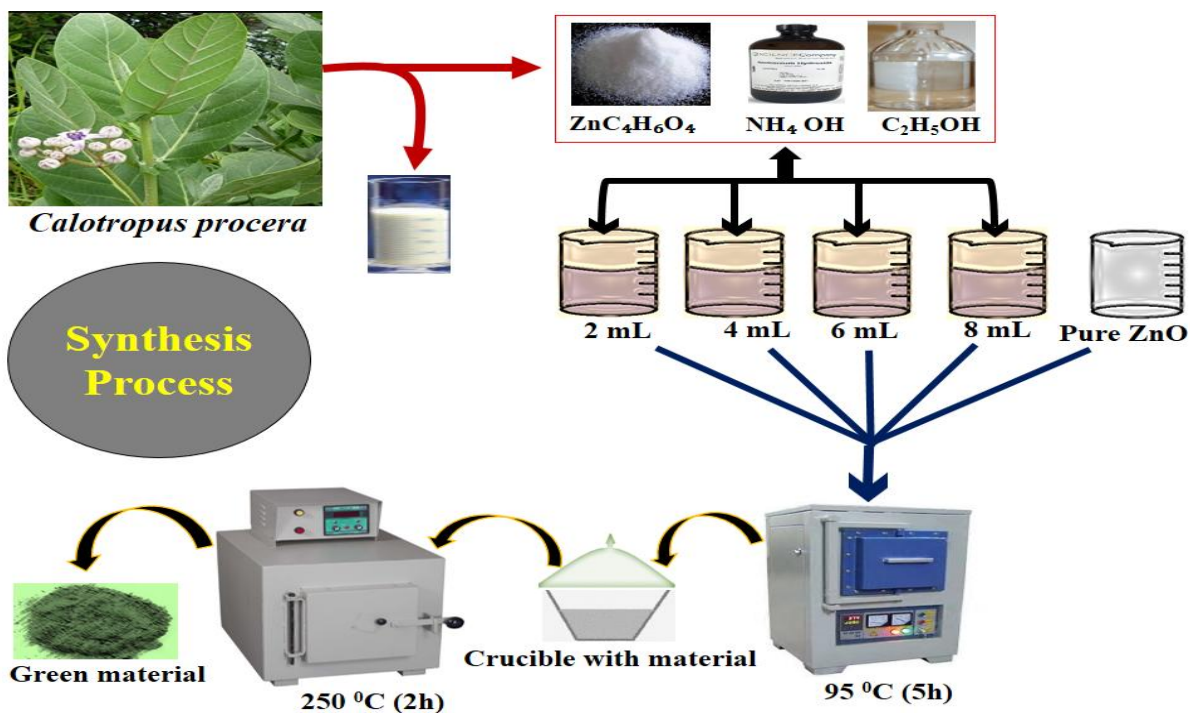
- [40]. M. Khatami, M.S. Nejad, S. Salari, P.G.N. Almani, Plant-mediated green synthesis of silver nanoparticles using *Trifolium resupinatum* seed exudate and their antifungal efficacy on *Neofusicoccum parvum* and *Rhizoctonia solani*. *IET Nanobiotechnol.* **10**, 237–243 (2016).
- [41]. L. Shiri, S. Rahmati, Z. Ramezani Nejad, M. Kazemi, Synthesis and characterization of bromine source immobilized on diethylenetriamine-functionalized magnetic nanoparticles: a novel, versatile and highly efficient reusable catalyst for organic synthesis. *Appl. Organo.Chem.* **31**, e3687 (2017).
- [42]. F. Ullah, S. Nasar Shah, W. Zaman, M. Zafar, M. Ahmad, A. Ayaz, A. Sohail, S. Saqib, Using palynomorphological characteristics for the identification of species of Alsinoideae (Caryophyllaceae): a systematic approach. *Grana.* **58**, 174–184 (2019).
- [43]. S. Hemmati, M. Baghayeri, S. Kazemi, H. Veisi, Biosynthesis of silver nanoparticles using oak leaf extract and their application for electrochemical sensing of hydrogen peroxide. *Appl. Organo.Chem.* **32**, e4537 (2018).
- [44]. B.C. Gibb, R.G. Chapman, J.C. Sherman, Synthesis of hydroxyl-footed cavitands. *J. Org. Chem.* **61**, 1505 (1996).
- [45]. M.G. Demissie, F.K. Sabir, G.D. Edossa, B.A. Gonfa. Synthesis of zinc oxide nanoparticles using leaf extract of *lippia adoensis* (koseret) and evaluation of its antibacterial activity. *Journal of Chemistry*, 1-9 (2020).
- [46]. S.W. Yun, Y. Shim, S.G. Cho, SINTERING BEHAVIOUR AND ELECTRICAL CHARACTERISTICS OF ZnO VARISTORS PREPARED BY PECHINI PROCESS. *J. Korean Ceram. Soc.*, **35**, 498-504 (1998).
- [47]. J.H. Ryu, C.S. Lim, K.H. Auh, Synthesis of ZnWO<sub>4</sub> Nanopowders by Polymerized complex Method. *Journal of the Korean Ceramic Society*, **39**, 321-326 (2002).
- [48]. R. Radhakrishnan, F.L.A. Khan, A. Muthu, A. Manokaran, J.S. Savarenathan, K. Kasinathan, Green synthesis of copper oxide nanoparticles mediated by aqueous leaf extracts of *Leucas aspera* and *Morinda tinctoria*. *Lett. Appl. Nanobiosci.* 102706–2714 (2021).

- [49]. A. Pugazhendhi, S.S. Kumar, M. Manikandan, M. Saravanani, Photocatalytic properties and antimicrobial efficacy of Fe doped CuO nanoparticles against the pathogenic bacteria and fungi. *Microb.Pathog.* **122**, 84–89 (2018).
- [50]. P.A. Luque-Morales, A. Lopez-Peraza, O.J. Nava-Olivas, G. Amaya-Parra, Y.A. Baez-Lopez, V.M. Orozco-Carmona, H.E. Garrafa-Galvez, M.D.J. Chinchillas-Chinchillas, ZnO semiconductor nanoparticles and their application in photocatalytic degradation of various organic dyes. *Materials*, **14**, 7537 (2021).
- [51]. M.A. Debeila, M.C. Raphulu, E. Mokoena, M. Avalos, V. Petranovskii, N.J. Coville, M.S. Scurrall, The influence of gold on the optical properties of sol–gel derived titania. *Materials Science and Engineering: A*, **396**, 70-76 (2005).
- [52]. T. Saad Algarni, N.A. Abduh, A. Al Kahtani, A. Aouissi, Photocatalytic degradation of some dyes under solar light irradiation using ZnO nanoparticles synthesized from *Rosmarinus officinalis* extract. *Green Chemistry Letters and Reviews*, **15**, 460-473 (2022).
- [53]. S. Chen, W. Zhao, W. Liu, S.J. Zhang, Preparation, characterization and activity evaluation of p-n junction photocatalyst p-NiO/n-ZnO. *J Sol-Gel Sci Technol*, **50**, 387–396 (2009).
- [54]. M.A. Bhatti, A.A. Shah, K.F. Almani, A. Tahira, S.E. Chalangar, A. dad Chandio, O. Nur, M. Willander, Z.H. Ibupoto, Efficient photo catalysts based on silver doped ZnO nanorods for the photo degradation of methyl orange. *Ceramics International*, **45**, 23289-23297 (2019).
- [55]. M.A. Bhatti, A. Tahira, K.F. Almani, A.L. Bhatti, B. Waryani, A. Nafady, Z.H. Ibupoto, Enzymes and phytochemicals from neem extract robustly tuned the photocatalytic activity of ZnO for the degradation of malachite green (MG) in aqueous media . *Research on Chemical Intermediates*, **47**, 1581-1599 (2021).
- [56]. Z. Zhao, Y. Zheng . *Science in China Series D: Earth Sciences*, **52**, 1295-1318 (2009).
- [57]. K. Sharma, R.K. Vyas, A.K. Dalai, Thermodynamic and kinetic studies of methylene blue degradation using reactive adsorption and its comparison with adsorption. *J. Chem. Eng. Data*. **62**, 3651–3662 (2017).

- [58]. T.H. Han, M.M. Khan, S. Kalathil, J. Lee, M.H. Cho, simultaneous enhancement of methylene blue degradation and power generation in a microbial fuel cell by gold nanoparticles. *Ind. Eng. Chem. Res.* **52**, 8174–8181 (2013).
- [59]. A.N. Rao, B. Sivasankar, V. Sadasiva, Kinetic study on the photocatalytic degradation of salicylic acid using ZnO catalyst. *Journal of hazardous materials*, **166** 1357-1361 (2009).
- [60]. N. Sobana, M. Swaminathan, The effect of operational parameters on the photocatalytic degradation of acid red 18 by ZnO. *Separation and purification technology*, **56**, 101-107 (2007).
- [61]. I.K. Konstantinou, T.A. Albanis, TiO<sub>2</sub>-assisted photocatalytic degradation of azo dyes in aqueous solution: kinetic and mechanistic investigations: a review. *Applied Catalysis B: Environmental*, **49**, 1-14 (2004).
- [62]. M.A. Behnajady, N. Modirshahla, R. Hamzavi, Kinetic study on photocatalytic degradation of CI Acid Yellow 23 by ZnO photocatalyst. *Journal of hazardous materials*, **133**, 226-232 (2006).
- [63]. R. Comparelli, E. Fanizza, M.L. Curri, P.D. Cozzoli, G. Mascolo, A. Agostiano, UV-induced photocatalytic degradation of azo dyes by organic-capped ZnO nanocrystals immobilized onto substrates. *Applied Catalysis B: Environmental*, **60**, 1-11 (2005).
- [64]. H. Li, S. Yin, Y. Wang, T. Sato, Efficient persistent photocatalytic decomposition of nitrogen monoxide over a fluorescence-assisted CaAl<sub>2</sub>O<sub>4</sub>: (Eu, Nd)/(Ta, N)-codoped TiO<sub>2</sub>/Fe<sub>2</sub>O<sub>3</sub>. *Applied Catalysis B: Environmental*, **132**, 487-492 (2013).
- [65]. B. Palanisamy, C.M. Babu, B. Sundaravel, S. Anandan, V. Murugesan, Sol–gel synthesis of mesoporous mixed Fe<sub>2</sub>O<sub>3</sub>/TiO<sub>2</sub> photocatalyst: application for degradation of 4-chlorophenol. *J Hazard Mater* **252**, 233–242 (2013).
- [66]. A. Muthuvel, M. Jothibas, C. Manoharan, S.J. Jayakumar, Synthesis of CeO<sub>2</sub>-NPs by chemical and biological methods and their photocatalytic, antibacterial and in vitro antioxidant activity. *Research on Chemical Intermediates*, **46**, 2705-2729 (2020).
- [67]. A. Muthuvel, M. Jothibas, V. Mohana, C. Manoharan, Green synthesis of cerium oxide nanoparticles using *Calotropis procera* flower extract and their photocatalytic degradation and antibacterial activity. *Inorganic Chemistry Communications*, **119**, 108086 (2020).
- [68]. J.C. Sin, J. Quek, S.M. Lam, H. Zeng, H. Lin, H. Li, K.O. Tham, A.R. Mohamed, J.W. Lim, Punica granatum mediated green synthesis of cauliflower-like ZnO and decorated

- with bovine bone-derived hydroxyapatite for expeditious visible light photocatalytic antibacterial, antibiofilm and antioxidant activities. *Journal of Environmental Chemical Engineering*, **9**, 105736 (2021).
- [69]. S.M. Lam, J.C. Sin, H. Zeng, H. Lin, H. Li, Y.Y. Chai, M.K. Choong, A.R. Mohamed, Green synthesis of Fe-ZnO nanoparticles with improved sunlight photocatalytic performance for polyethylene film deterioration and bacterial inactivation. *Materials Science in Semiconductor Processing*, **123**, 105574 (2021).
- [70]. Y.H. Chin, J.C. Sin, S.M. Lam, H. Zeng, H. Lin, H. Li, L. Huang, A.R. Mohamed, 3-D/3-D Z-Scheme Heterojunction Composite Formed by Marimo-like Bi<sub>2</sub>WO<sub>6</sub> and Mammillaria-like ZnO for Expeditious Sunlight Photodegradation of Dimethyl Phthalate. *Catalysts*, **12**, 1427 (2022).
- [71]. Y.H. Chin, J.C. Sin, S.M. Lam, H. Zeng, H. Lin, H. Li, A.R. Mohamed, 0-D/3-D heterojunction composite constructed by decorating transition metal oxide nanoparticle on peony-like ZnO hierarchical microstructure for improved photodegradation of palm oil mill effluent. *Optik*, **260**, 169098 (2022).
- [72]. S.M. Lam, K.C. Chew, J.C. Sin, H. Zeng, H. Lin, H. Li, J.W. Lim, A.R. Mohamed, Ameliorated photodegradation performance of polyethylene and polystyrene films incorporated with ZnO-PVP catalyst. *Journal of Environmental Chemical Engineering*, **10**, 107594 (2022).
- [73]. K. Elumalai. S. Velmurugan. Green synthesis, characterization and antimicrobial activities of zinc oxide nanoparticles from the leaf extract of *Azadirachta indica* (L.) *Appl. Surf. Sci.* **345**, 329–36 (2015).
- [74]. J. Osuntokun, D.C. Onwudiwe, E.E. Ebenso, Green synthesis of ZnO nanoparticles using aqueous *Brassica oleracea* L. var. *italica* and the photocatalytic activity. *Green chemistry letters and reviews*, **12**, 444-457(2019).
- [75]. M.H. Kahsay, Synthesis and characterization of ZnO nanoparticles using aqueous extract of *Becium grandiflorum* for antimicrobial activity and adsorption of methylene blue. *Applied Water Science*, **11**, 45 (2021)

- [76]. M.J. Haque, M.M. Bellah, M.R. Hassan, S. Rahman, Synthesis of ZnO nanoparticles by two different methods & comparison of their structural, antibacterial, photocatalytic and optical properties. *Nano Express*, **1**, 0007 (2020).
- [77]. Y.C. Liu, J. Li, J. Ahn, J. Pu, E.J. Rupa, Y. Huo, D.C. Yang, Biosynthesis of zinc oxide nanoparticles by one-pot green synthesis using fruit extract of *Amomum longiligulare* and its activity as a photocatalyst. *Optik*, **218**, 165245 (2020).
- [78]. M.P. Kumar, D. Suresh, H. Nagabhushana, S.C. Sharma, Beta vulgaris aided green synthesis of ZnO nanoparticles and their luminescence, photocatalytic and antioxidant properties. *Eur. Phys. J. Plus*, **130**, 109 (2015).
- [79]. J.K. Park, E.J. Rupa, M.H. Arif, J.F. Li, G. Anandapadmanaban, J.P. Kang, M. Kim, J.C. Ahn, R. Akter, D.C. Yang, S.C. Kang, Synthesis of zinc oxide nanoparticles from *Gynostemma pentaphyllum* extracts and assessment of photocatalytic properties through malachite green dye decolorization under UV illumination-A Green Approach. *Optik*, **239**, 166249 (2021).
- [80]. F.M. Albarakaty, M.I. Alzaban, N.K. Alharbi, F.S. Bagrwan, A.R. Abd El-Aziz, M.A. Mahmoud, Zinc oxide Nanoparticles, Biosynthesis, characterization and their potent photocatalytic degradation, and antioxidant activities. *Journal of King Saud University-Science*, **35**, 102434 (2023).
- [81]. A. El Golli, M. Fendrich, N. Bazzanella, C. Dridi, A. Miotello, M. Orlandi, Wastewater remediation with ZnO photocatalysts: Green synthesis and solar concentration as an economically and environmentally viable route to application. *Journal of Environmental Management*, **286**, 112226 (2021).
- [82]. S.M. Rao, S. Kotteswaran, A.M. Visagamani, Green synthesis of zinc oxide nanoparticles from *camellia sinensis*: Organic dye degradation and antibacterial activity. *Inorganic Chemistry Communications*, **134**, 108956 (2021).



**Scheme 1:** Preparation of ZnO nanostructures using milky sap of CP from leaves, stem and flowers using solvothermal process followed calcination in the air

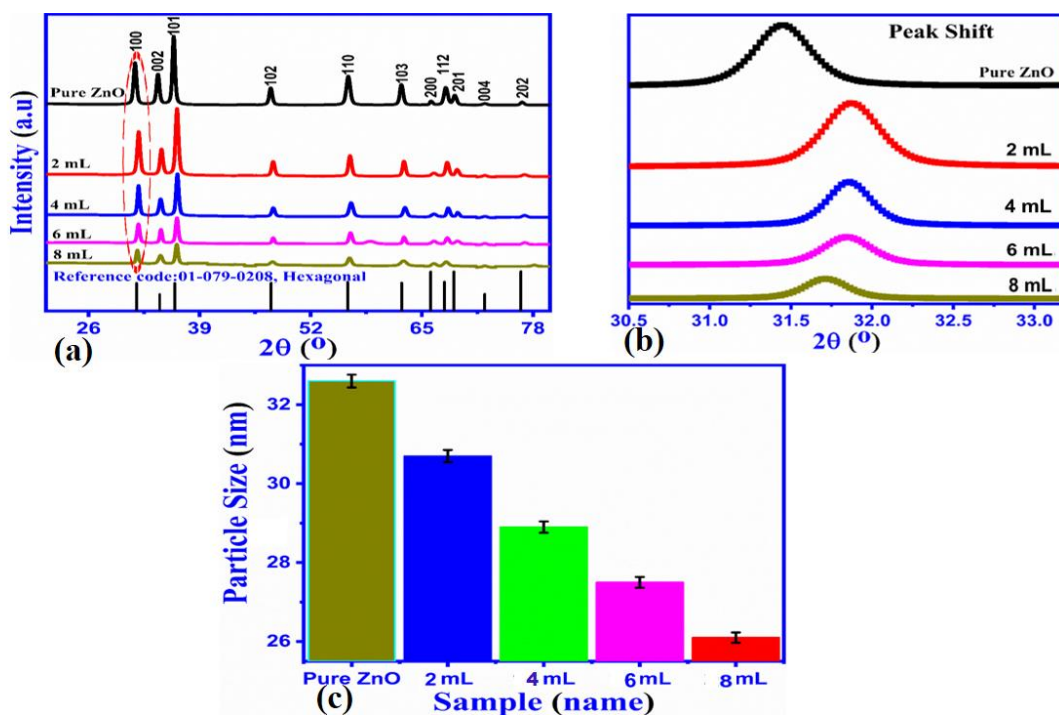


**Figure 1:** (a) XRD patterns of pure ZnO and biosynthesized ZnO samples with milky sap of CP (b), (b) shift at higher angle localized at (002) (c) calculated average crystallite size

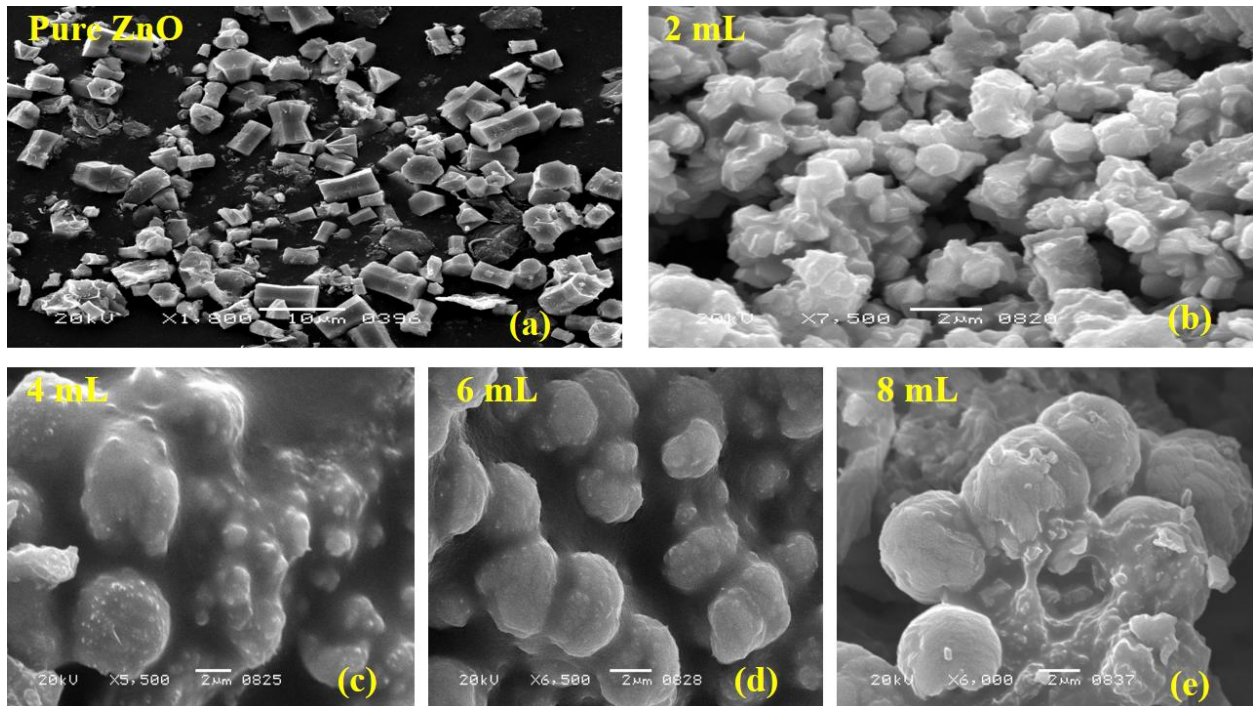
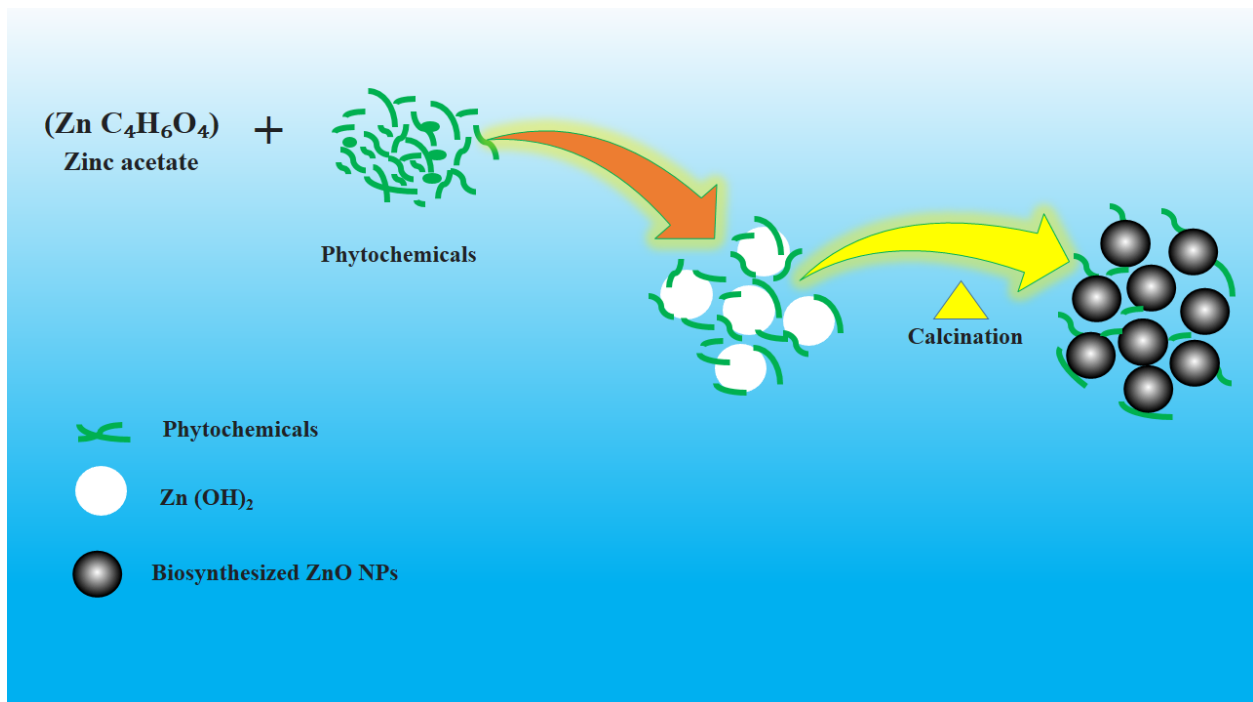


**Figure 2:** SEM images (a) pure ZnO, (b-e) ZnO samples prepared with different volumes of milky sap of CP like 2 mL, 4 mL, 6 mL, 8 mL



**Scheme 2.** Typical proposed mechanism of formation of Biosynthesized ZnO with *Calotropis procera* extract.

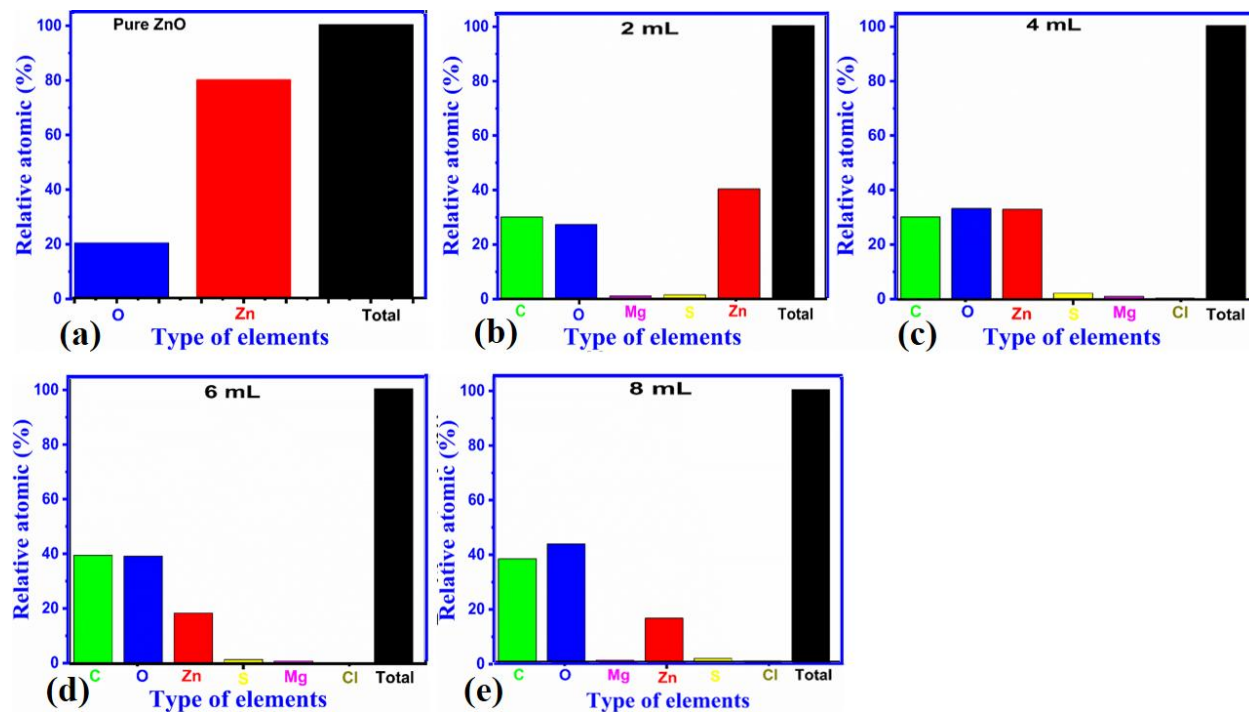


**Figure 3:** EDX (a) pure ZnO, (b-e) biosynthesized ZnO samples with different volumes of milky sap of CP such as 2 mL, 4 mL, 6 mL and 8 mL

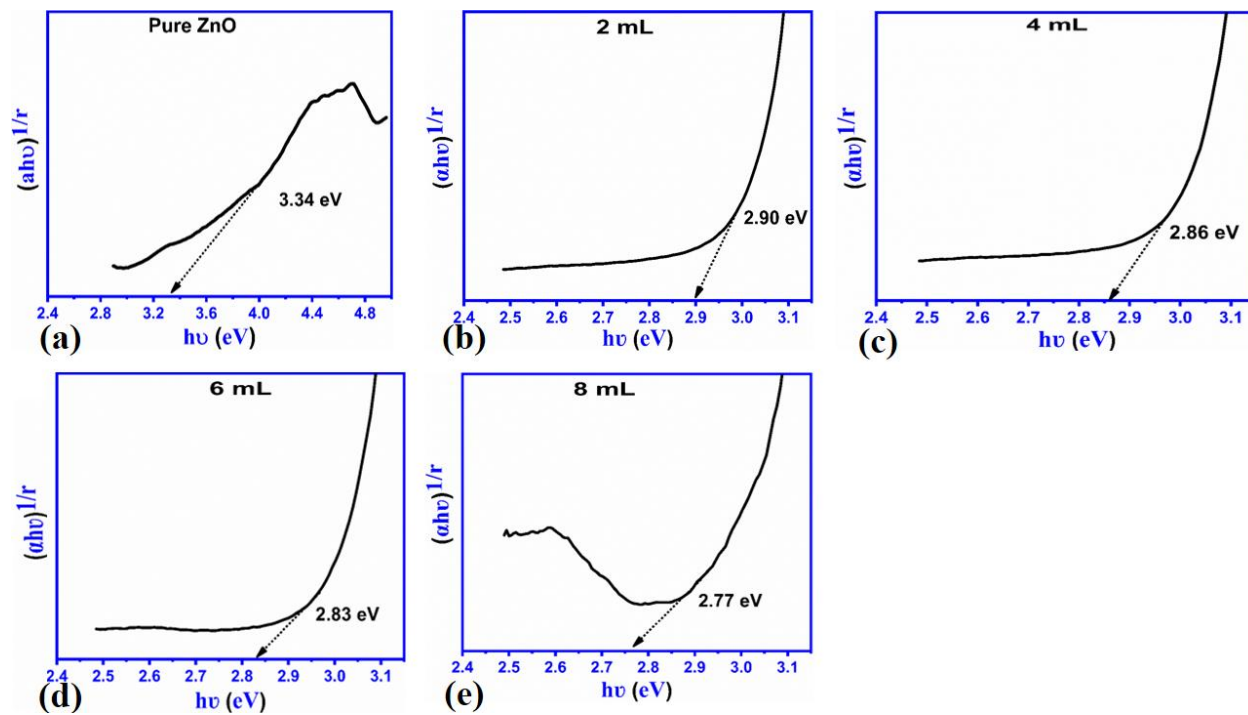


**Figure 4:** Kubelka–Munk plots of (a) pure ZnO and biosynthesized ZnO samples grown with different volume of milky sap of CP like 2, 4, 6 and 8 mL

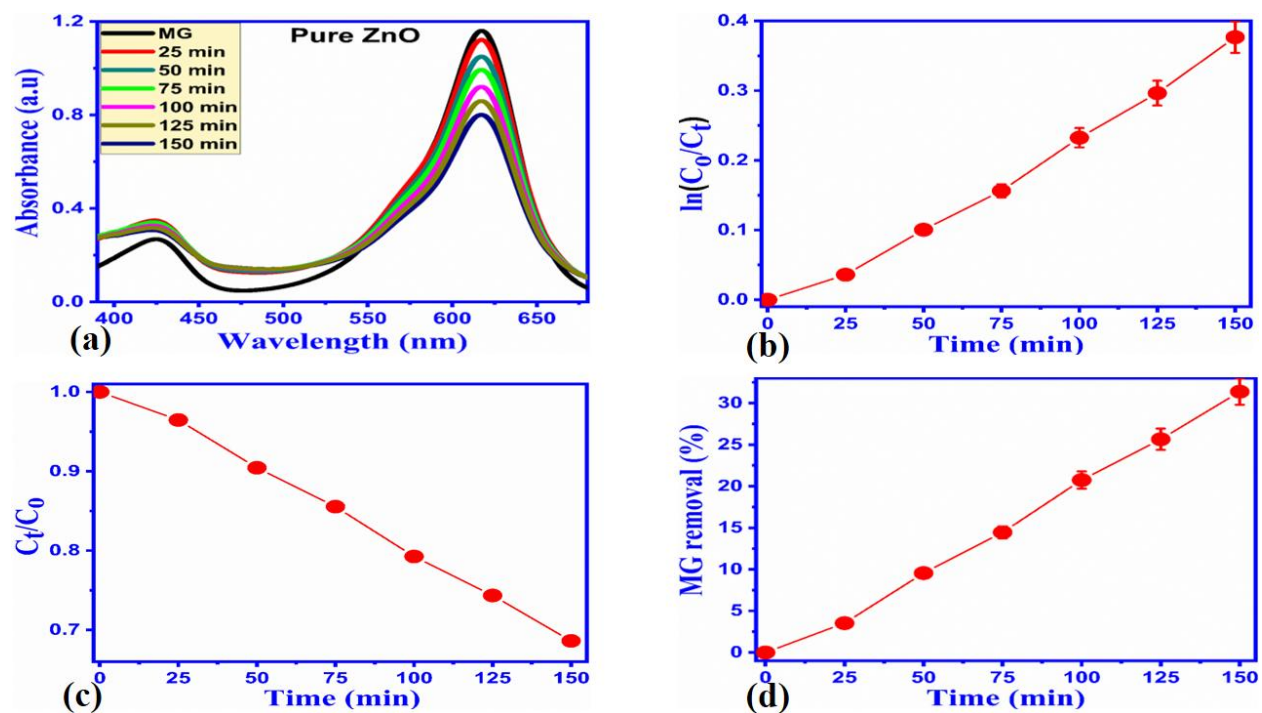


**Figure 5:** (a) UV-vis absorbance for the decomposition of MG under ultra violet light exposure using pure ZnO, (b, c) Kinetics study of MG degradation (d) removal percentage of MG using pure ZnO.

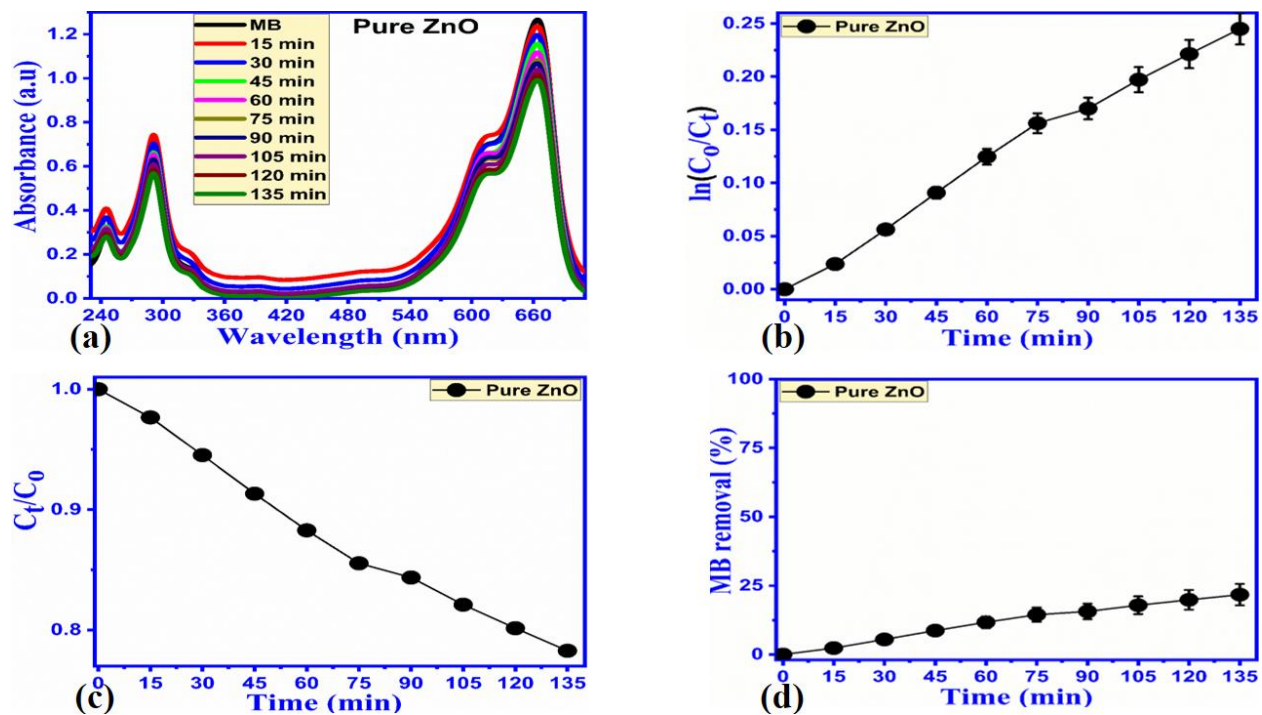


Figure 6: (a) UV-vis absorbance for decomposition of MB under ultra violet light exposure using pure ZnO, (b, c) Kinetics study of photodegradation of MB, (d) percent degradation efficiency of MB

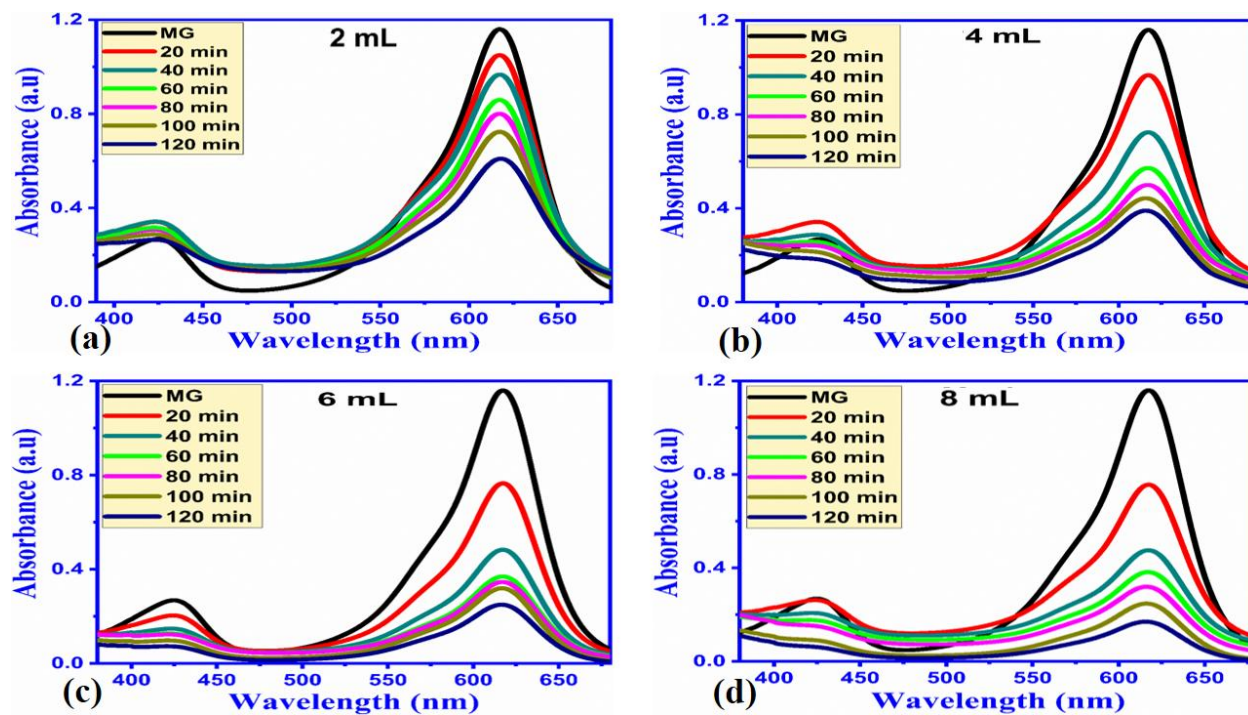
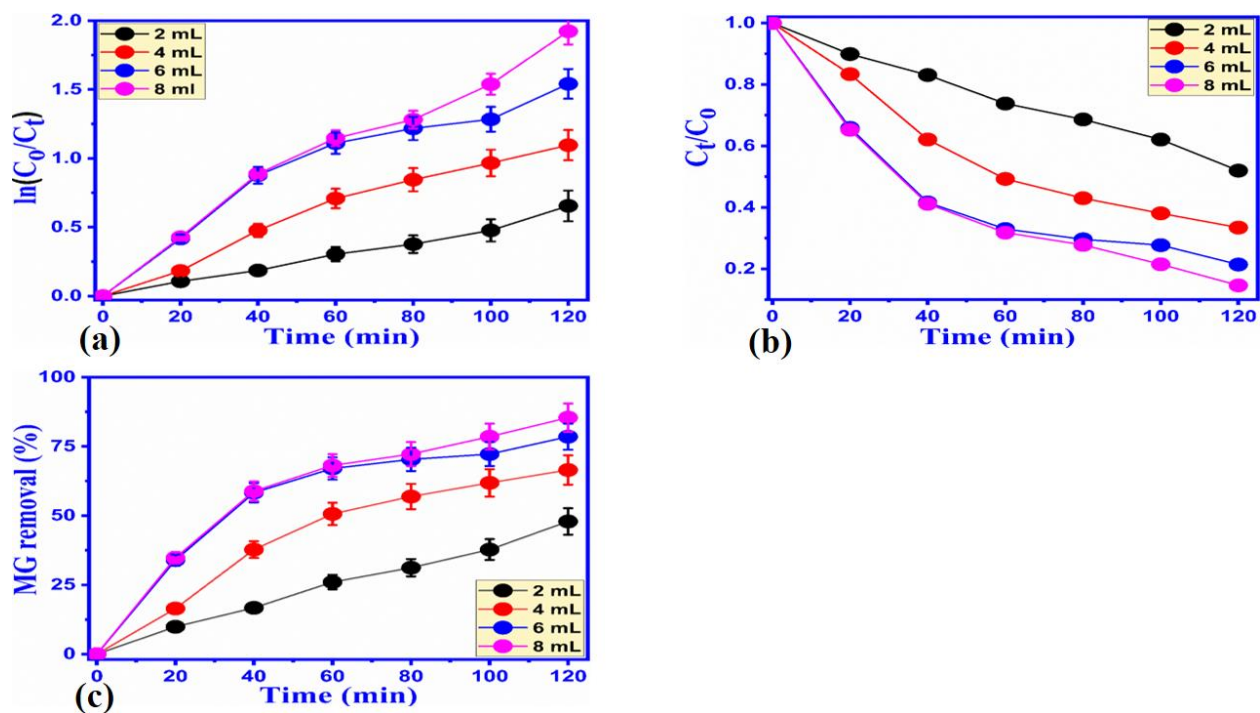
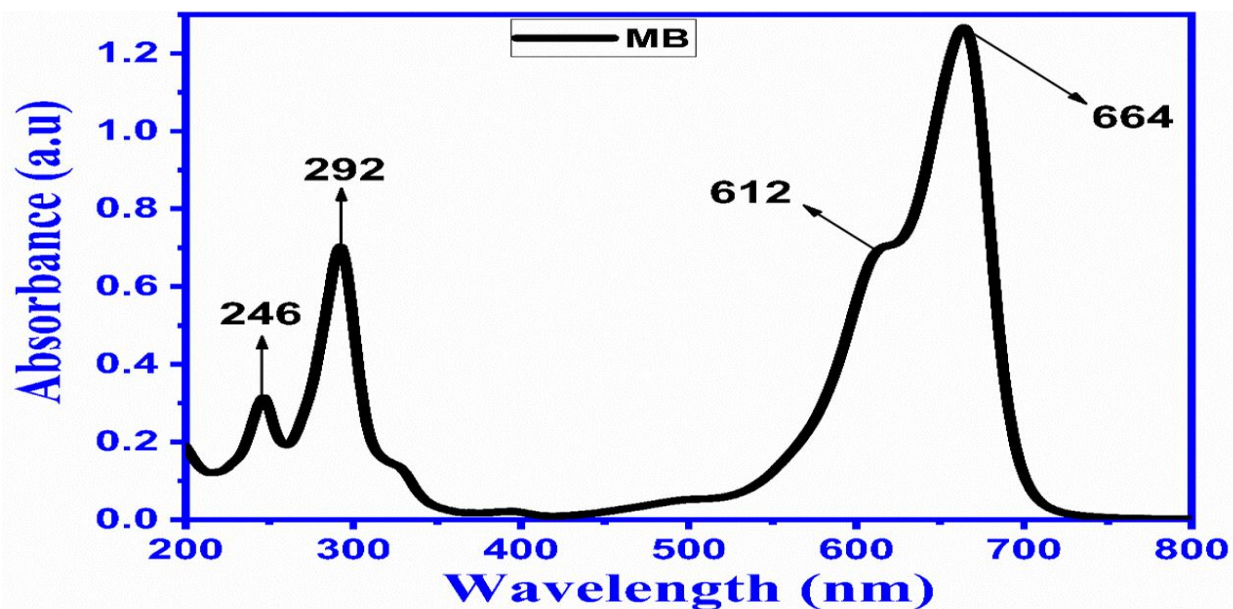


Figure 7. (a-d) UV-vis absorbance for decomposition of MG dye under ultra violet light using ZnO nanostructures prepared with different volumes of milky sap of CP like 2, 4, 6 and 8 mL



**Figure 8:** (a, b) Kinetics study of MG using ZnO nanostructures prepared with different volumes of milky sap of CP like 2, 4, 6 and 8 mL, (c) degradation efficiency of MG



**Figure 9:** Absorbance spectrum of MB dye

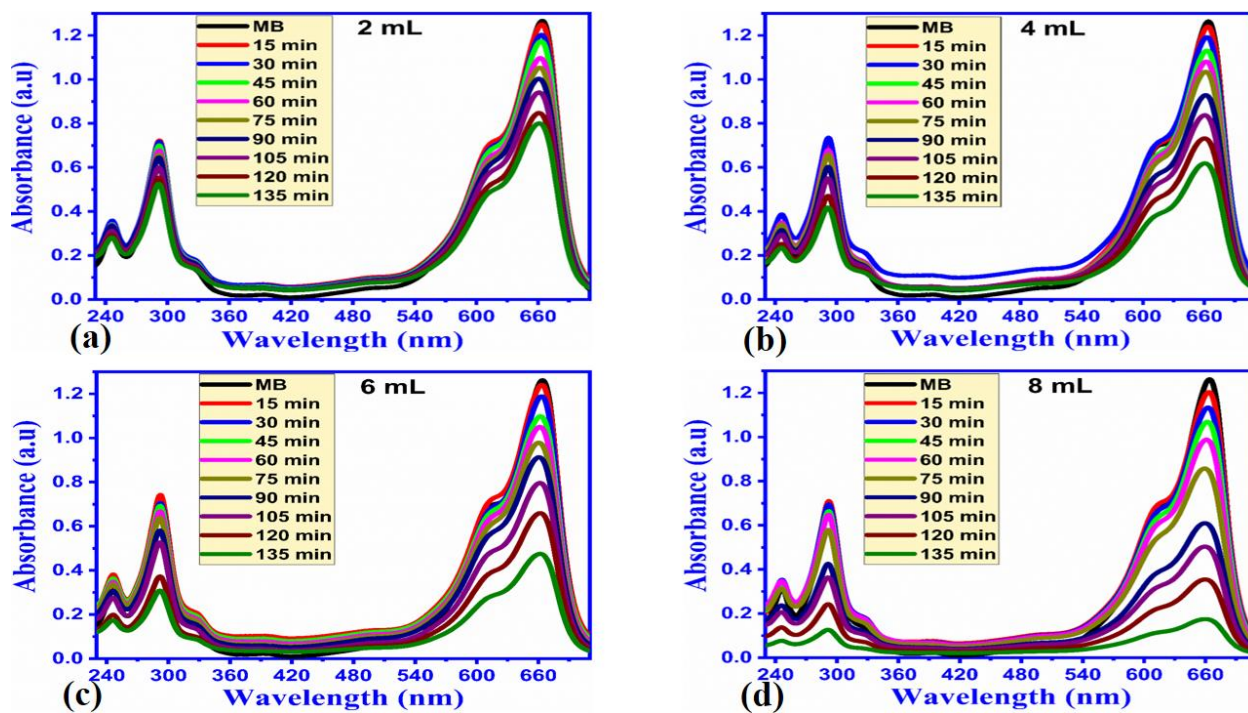


**Figure 10:** (a-d) UV-vis absorbance for decomposition of MB dye under ultra violet light using ZnO nanostructures prepared with different volumes of milky sap of CP like 2, 4, 6 and 8 mL

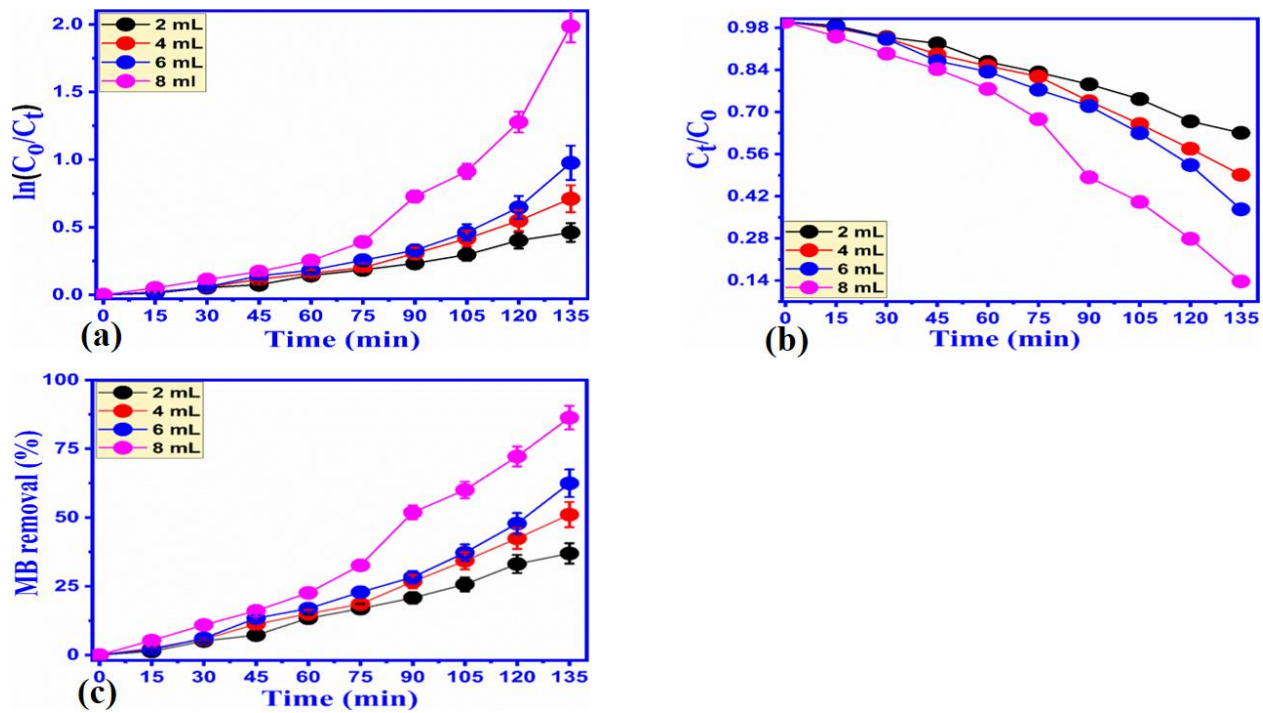


**Figure 11:** (a, b) Kinetics study of MB using ZnO nanostructures prepared with different volumes of milky sap of CP like 2, 4, 6 and 8 mL, (c) degradation efficiency of MB

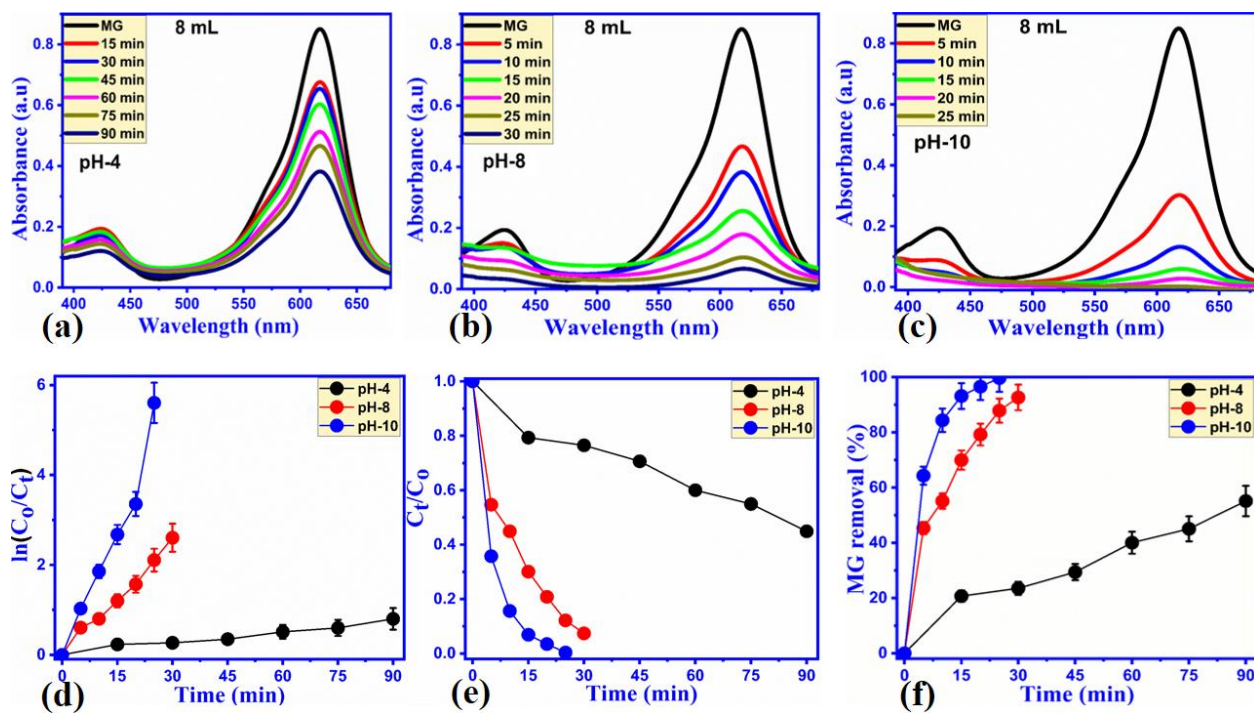


**Figure 12:** (a-c) UV-vis absorbance for decomposition of MG under ultra violet light exposure using ZnO sample prepared with 8 mL of milky sap of CP in different pH values like 4, 8 and 10, (d-e) Kinetics study of MG under various pH values, (f) degradation efficiency of MG at 4, 8 and 10 pH values

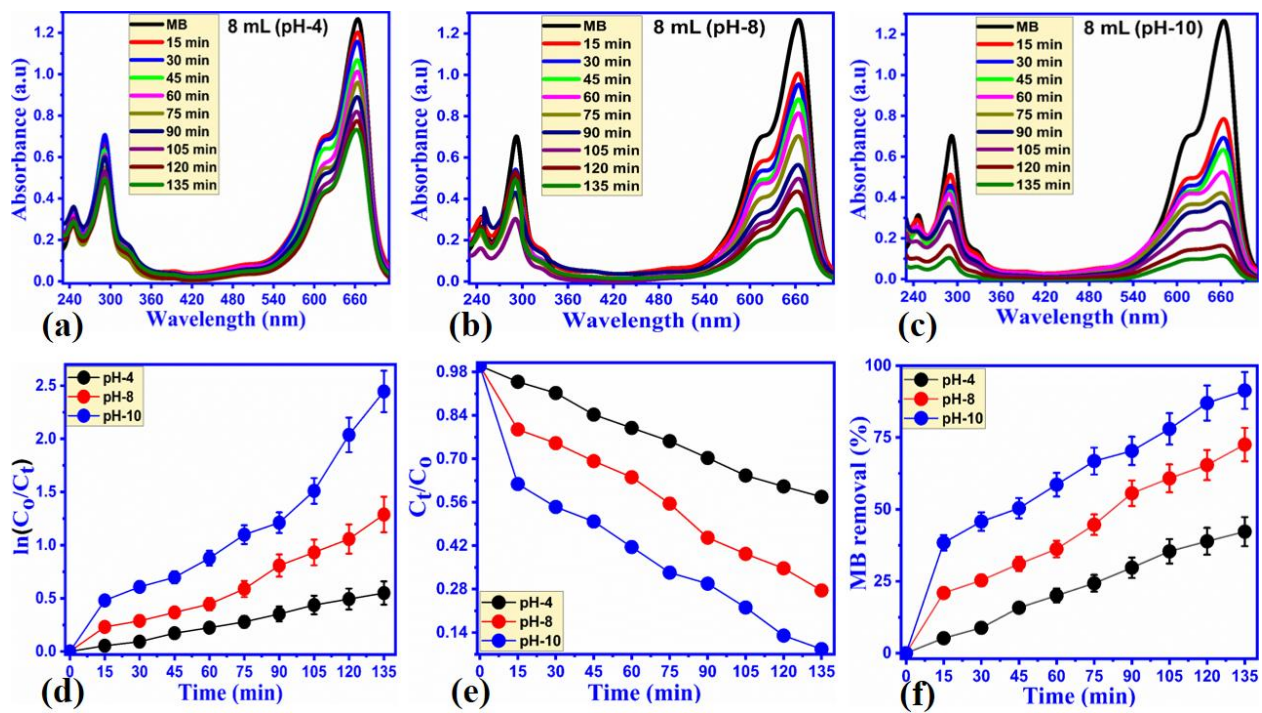
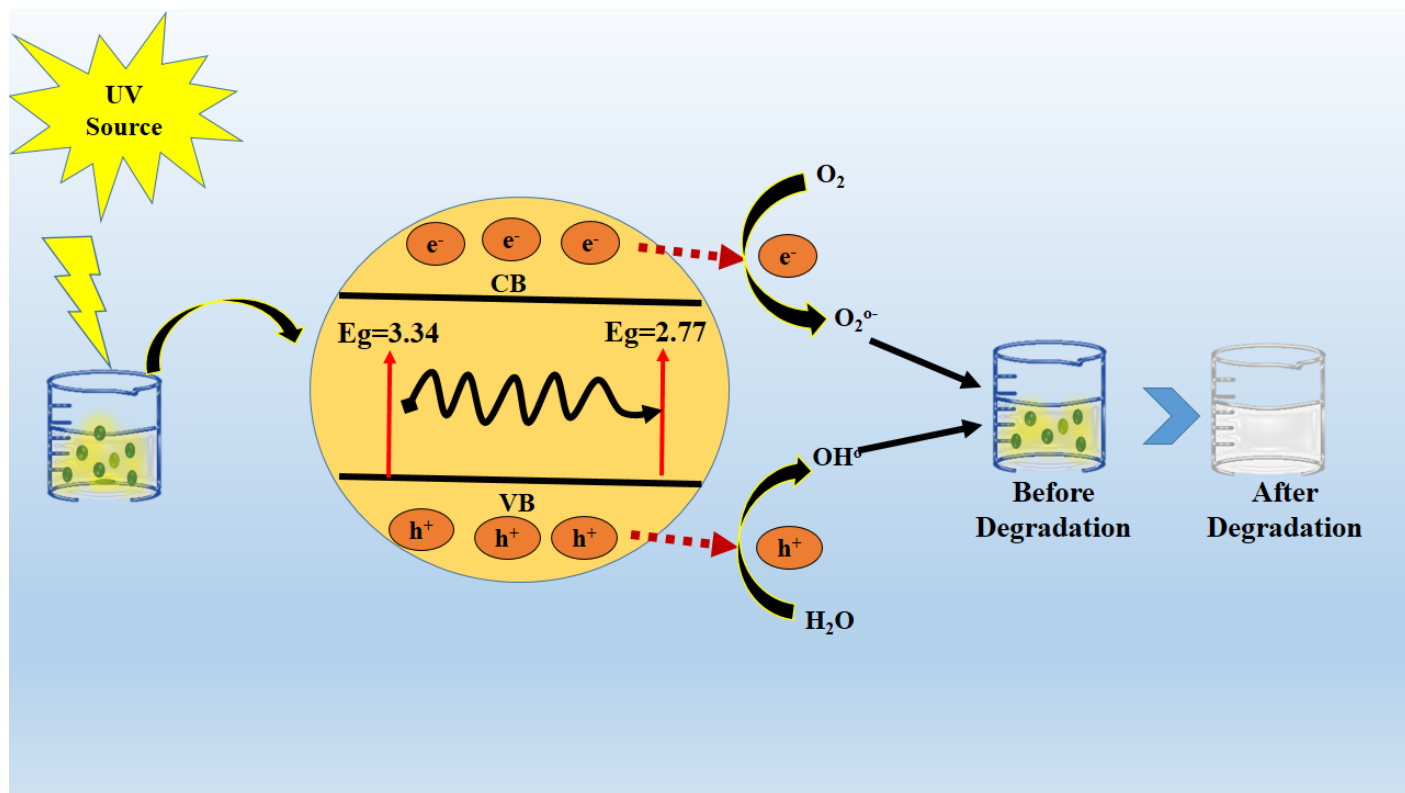


**Figure 13:** (a-c) UV-vis absorbance for decomposition of MB under ultra-violet light exposure using ZnO sample prepared with 8 mL of milky sap of CP in different pH values like 4, 8 and 10, (d-e) Kinetics study of MB under various pH values, (f) degradation efficiency of MB at 4, 8 and 10 pH values



**Scheme 3:** General photodegradation mechanism on the ZnO surface under the illumination of UV light

**Table 1:** Different parameters of biosynthesized ZnO nanoparticles

Samples	Band gap energy (eV)	Rate constant (K), min <sup>-1</sup> MG	Rate constant (K), min <sup>-1</sup> MB	Particle Size
Pure ZnO	3.34	0.00255	0.00184	32.6
2 mL	2.90	0.00517	0.00384	30.7
4 mL	2.86	0.00933	0.00506	28.9
6 mL	2.83	0.01196	0.00639	27.5
8 mL	2.77	0.01497	0.01304	26.1
Sample	Rate constant (K), min <sup>-1</sup> MG	Rate constant (K), min <sup>-1</sup> MG	Rate constant (K), min <sup>-1</sup> MG	
	pH-4	pH-8	pH-10	
8 mL	0.00805	0.08277	0.20468	
Sample	Rate constant (K), min <sup>-1</sup> MB	Rate constant (K), min <sup>-1</sup> MB	Rate constant (K), min <sup>-1</sup> MB	
	pH-4	pH-8	pH-10	
8 mL	0.00418	0.00892	0.01584	

**Table 2.** Comparative list of ZnO NPs synthesized using various plants and their dye removal percentages (%).

Material Used	Biological entity	Synthesis method	Pollutant	Dye removal (%)	Time (min)	Ref.
ZnO	Azadirachta indica	eco-friendly method	MB	82%	120	73
ZnO	<i>Brassica oleracea</i> L. var. <i>italica</i>	calcination process	MB	74%	180	74
ZnO	<i>Becium grandiflorum</i>	green synthesis Method	MB	69 %	200	75
ZnO	Azadirachta Indica	Sol-gel and biosynthesis	MB	82.2%	200	76
ZnO	<i>Amomum longiligulare</i>	co-precipitation method	MG/MB	38% & 66%	60	77
ZnO	Beta vulgaris	solution combustion synthesis	MB	80%	150	78
ZnO	<i>Gynostemma</i>	ecofriendly	MG	89%	180	79

	<i>pentaphyllum</i>	green <u>synthesis</u> method				
ZnO	<i>Camellia sinensis</i>	green-synthesis Method	MB	80 %	120	80
ZnO	Allium Sativum	green <u>synthesis</u> method	MB	73%	120	81
ZnO	<i>Camellia sinensis</i> powder	Combustion	MO	80 %	180	82
ZnO	Calotropis procera	Hydrothermal	MG/MB	85.3% & 86.3%	120/135	Present work